Åbo Akademi University

Jawad Sarfraz

Development and Characterization of Thin Printed Films for Gas Sensing Applications

Laboratory of Physical Chemistry
Center for Functional Materials
Faculty of Science and Engineering

Development and Characterization of Thin Printed Films for Gas Sensing Applications

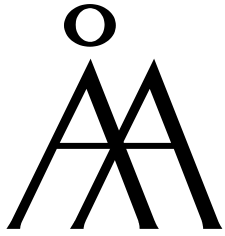

Jawad Sarfraz

Laboratory of Physical Chemistry

Center for Functional Materials

Faculty of Science and Engineering

Åbo Akademi University

Åbo, Finland

2015

Supervised by

Professor Jouko Peltonen
Laboratory of Physical Chemistry
Åbo Akademi University, Åbo, Finland

Co-supervised by

Dr. Petri Ihalainen
Laboratory of Physical Chemistry
Åbo Akademi University, Åbo, Finland

Reviewed by

Professor Kalle Levon
Department of Chemical and Biomolecular Engineering
New York University, United States

and

Professor Michael Tiemann
Department of Chemistry
University of Paderborn, Germany

Opponent

Professor Kalle Levon
Department of Chemical and Biomolecular Engineering
New York University, United States

ISBN 978-952-12-3251-0 (PRINT)
ISBN 978-952-12-3252-7 (PDF)
Painosalama Oy – Turku, Finland 2015

PREFACE

The research work presented in this PhD thesis was performed at the Laboratory of Physical Chemistry, Åbo Akademi University.

I am very thankful to Professor Mika Lindén and Professor Jouko Peltonen for hiring me at the Laboratory of Physical Chemistry and giving me the opportunity to work in your groups. I am grateful for your guidance, support and useful discussions.

Special thanks to Dr. Petri Ihalainen for the helpful supervision of my research, the invaluable advices and the interesting discussions we have shared during these years. I would also like to thank all of my coauthors and colleagues for being around and making this work possible. It has been gratifying working with all of you. Especially I want to thank Björn Törngren for being a wonderful friend during all these years.

Furthermore, I am honored to have Professor Kalle Levon (New York University) and Professor Michael Tiemann (University of Paderborn) as the reviewers of this thesis.

The Finnish Funding Agency for Technology and Innovation (TEKES), Academy of Finland and the European Regional Development Fund (ERDF) are acknowledged for the financial support.

Finally, I am deeply thankful to my whole family for your patience and support during all these years.

CONTENTS

ABSTRACT

The monitoring and control of hydrogen sulfide (H_2S) level is of great interest for a wide range of application areas including food quality control, defense and anti-terrorist applications and air quality monitoring e.g. in mines. H_2S is a very poisonous and flammable gas. Exposure to low concentrations of H_2S can result in eye irritation, a sore throat and cough, shortness of breath, and fluid retention in the lungs. These symptoms usually disappear in a few weeks. Long-term, low-level exposure may result in fatigue, loss of appetite, headache, irritability, poor memory, and dizziness. Higher concentrations of 700 - 800 ppm tend to be fatal. H_2S has a characteristic smell of rotten egg. However, because of temporary paralysis of olfactory nerves, the smelling capability at concentrations higher than 100 ppm is severely compromised.

In addition, volatile H_2S is one of the main products during the spoilage of poultry meat in anaerobic conditions. Currently, no commercial H_2S sensor is available which can operate under anaerobic conditions and can be easily integrated in the food packaging. This thesis presents a step-wise progress in the development of printed H_2S gas sensors. Efforts were made in the formulation, characterization and optimization of functional printable inks and coating pastes based on composites of a polymer and a metal salt as well as a composite of a metal salt and an organic acid. Different processing techniques including inkjet printing, flexographic printing, screen printing and spray coating were utilized in the fabrication of H_2S sensors. The dispersions were characterized by measuring turbidity, surface tension, viscosity and particle size. The sensing films were characterized using X-ray photoelectron spectroscopy, X-ray diffraction, atomic force microscopy and an electrical multimeter.

Thin and thick printed or coated films were developed for gas sensing applications with the aim of monitoring the H_2S concentrations in real life applications. Initially, a H_2S gas sensor based on a composite of polyaniline and metal salt was developed. Both aqueous and solvent-based dispersions were developed and characterized. These dispersions were then utilized in the fabrication of roll-to-roll printed H_2S gas sensors. However, the humidity background, long term instability and comparatively lower detection limit made these sensors less favourable for real practical applications. To overcome these problems, copper acetate based sensors were developed for H_2S gas sensing. Stable inks with excellent printability were developed by tuning the surface tension, viscosity and particle size. This enabled the formation of inkjet-printed high quality copper acetate films with excellent sensitivity towards H_2S. Furthermore, these sensors showed negligible humidity effects and improved selectivity, response time, lower limit of detection and coefficient of variation. The lower limit of detection of copper acetate based sensors was further improved to sub-ppm level by incorporation of catalytic gold nano-particles and subsequent plasma treatment of the sensing film. These sensors were further integrated in an inexpensive wirelessly readable RLC-

circuit (where R is resistor, L is inductor and C is capacitor). The performance of these sensors towards biogenic H_2S produced during the spoilage of poultry meat in the modified atmosphere package was also demonstrated in this thesis. This serves as a proof of concept that these sensors can be utilized in real life applications.

SVENSK SAMMANFATTNING

Att kunna mäta och kontrollera halten svavelväte (H_2S) är av stort intresse inom många olika områden såsom kvalitetskontroll av mat, försvar och anti-terrorism, samt för att övervaka luftkvaliteten i gruvor. H_2S är en mycket giftig och brandfarlig gas. Exponering för låga halter H_2S-gas kan ge upphov till ögonsveda, halsont och hosta, andnöd och vätskeansamling i lungorna. Dessa symptom försvinner vanligen inom några veckor. En längre tids exponering kan resultera i trötthet, aptitlöshet, huvudvärk, minnesförlust och yrsel. Högre koncentrationer (700 - 800 ppm) tenderar att vara dödlig. Lukten av H_2S-gas brukar beskrivas som ruttna ägg, men på grund av en tillfällig förlamning av luktsinnet vid koncentrationer högre än 100 ppm, kan exponering förekomma utan att det märks. H_2S är också den gas som i huvudsak frigörs vid nedbrytning av fjäderfäkött under anaeroba förhållanden. Dock finns för närvarande ingen kommersiell H_2S-sensor som kan verka under anaeroba förhållanden och enkelt integreras i livsmedelsförpackningar.

Målet med detta arbete var att utveckla en kostnadseffektiv H_2S-gassensor med förbättrade sensoregenskaper. Kommersiellt tillgängliga material modifierades och optimerades för tryckbarhet och mätning av H_2S. Tryckbarheten är viktigt eftersom den möjliggör massproduktion av sensorer samt sänker kostnaderna för varje sensor.

Till en början framställdes filmer med en blandning av deprotonerad polyanilin (PANI) och kopparklorid (CC), med så kallad ”drop-casting” teknik, på papper där silverelektroder tryckts med inkjet-teknik. Dessa filmer gav stor förändring i resistans ($>10^3$) då de exponerades för låga koncentrationer H_2S (10 ppm) vid rumstemperatur. Denna stora förändring i resistans visades uppstå från bildandet av kopparsulfid (CuS) och samtidig protonering av PANI. PANI nanofibrer har tidigare använts för sensorfilmer för att förbättra detektionen av H_2S-gas med hjälp av dess stora ytarea. Vi har i denna studie demonstrerat att liknande resultat kan uppnås med konventionell PANI genom att optimera koncentrationerna av PANI och metallsalt, samt använda ett poröst substrat såsom papper.

Vidare demonstrerades en fullt printbar H_2S-gassensor bestående av en vattenbaserad dispersion av PANI och CC. Silktryckning (serigrafi) eller så kallad ”spray bestrykning” användes för att belägga sensormaterialet på silverelektroder. Känsligheten för H_2S-gas i förhållande till pH och koncentration av metallsalt optimerades. Dessa tryckta filmer uppvisade klart förbättrad känslighet för H_2S-gas jämfört med filmerna framställda med drop-casting teknik. Ett problem var dock PANI/CC dispersionens ostabilitet vid det optimerade pH-värdet. Slutsatsen drogs att de optimerade PANI/CC dispersionerna (optimal med avseende på känsligheten för H_2S) inte var lämpliga för rulle-till-rulle tryckning.

Studien fortsatte med att förbättra stabiliteten för PANI/CC dispersionen. För detta ändamål användes en blandning av citronsyra (CA) och CC istället för endast CC. Genom att tillsätta CA förbättrades totalt sätt stabiliteten för dispersionen utan att påverka känsligheten för H_2S. Med denna stabila dispersion trycktes filmer med flexografi rulle-till-rulle teknik, varefter filmernas känslighet för H_2S kontrollerades.

Det visade sig att användningen av sensorer baserade på PANI i tillämpningar i verkliga livet är begränsade på grund av dess höga känslighet för fukt och ostabilitet under en längre period. Dessa orsaker gjorde att en fullt tryckbar H_2S-sensor baserad på kopparacetat (CuAc) demonstrerades. Denna sensor gav flerfaldigt större förändring i resistans ($>10^8$) då den exponerades för 10 ppm H_2S-gas vid rumstemperatur. För att vidare optimera sensorn studerades inverkan av olika lösningsmedel, filmtjocklek och substrat (absorberande och icke-absorberande). Den stora förändring i resistans visades bero på omvandlingen av isolerande CuAc-partiklar till semi-metalliska Cu_2S-partiklar.

Den tryckta CuAc-baserade H_2S-sensorn uppvisade utmärkt känslighet mot H_2S-gas och var stabil under en längre period. Påverkan av fukt och andra gaser var försumbar. Det konstaterades att sensorn kan användas för kvantitativ detektering av H_2S inom intervallet 1 - 20 ppm. Sensorn kunde vidare avsevärt förbättras genom att tillsätta katalytiska guldnanopartiklar och plasmabehandla filmytan. Med denna modifierade sensor kunde sub-ppm nivåer av H_2S detekteras vid rumstemperatur.

Slutligen demonstrerades trådlös detektion av biogen H_2S från nedbrytning av fjäderfäkött med CuAc-baserade sensorn. Sensorn integrerades i en RLC-krets och genererade en trådlös signal vid kontakt med H_2S-gas. Det observerades att vid hög fuktighet degraderar silverelektroderna om de exponeras för H_2S-gas under en längre tid (> 2-3 h) och är därför endast lämpliga för kortare exponeringstider.

LIST OF INCLUDED PUBLICATIONS

I **J. Sarfraz**, D. Tobjork, R. Osterbacka, M. Lindén. **Low-cost hydrogen sulfide gas sensor on paper substrates: fabrication and demonstration**. Sensors Journal, IEEE, 12 (2012) 1973 - 1978.

II **J. Sarfraz**, P. Ihalainen, A. Määttänen, J. Peltonen, M. Lindén. **Printed hydrogen sulfide gas sensor on paper substrate based on polyaniline composite**. Thin Solid Films, 534 (2013) 621 - 628.

III **J. Sarfraz**, P. Ihalainen, A. Määttänen, R. Bollström, T. Gulin-Sarfraz, J. Peltonen, M. Lindén. **Stable ink dispersions suitable for roll-to-roll printing with sensitivity towards hydrogen sulphide gas**. Colloids and Surfaces A: Physicochemical Engineering Aspects, 460 (2014) 401 - 407.

IV **J. Sarfraz**, A. Määttänen, P. Ihalainen, M. Keppeler, M. Lindén, J. Peltonen. **Printed copper acetate based H_2S sensor on paper substrate**. Sensors and Actuators B: Chemical, 173 (2012) 868 - 873.

V **J. Sarfraz**, P. Ihalainen, A. Määttänen, T. Gulin, J. Koskela, C.-E. Wil´en, A. Kilpelä and J. Peltonen. **A printed H_2S sensor with electro-optical response**. Sensors and Actuators B: Chemical, 191 (2014) 821 - 827.

VI **J. Sarfraz**, A. Määttänen, B. Törngren, M. Pesonen, J. Peltonen and P. Ihalainen. **Sub-ppm electrical detection of hydrogen sulfide gas at room temperature based on printed copper acetate-gold nanoparticle composite films**. RSC Advances, 5 (2015) 13525 - 13529.

VII J. Koskela, **J. Sarfraz**, P. Ihalainen, A. Määttänen, P. Pulkkinen, H. Tenhu, T. Nieminen, A. Kilpelä and J. Peltonen. **Monitoring the quality of raw poultry by detecting hydrogen sulphide with printed sensors**. Sensors and Actuators B: Chemical, 218 (2015) 89 - 96.

CONTRIBUTION OF THE AUTHOR

(I) The author was responsible for sample preparation, analysis of results and writing the first draft. The inkjet-printing of electrodes and XPS measurements were performed by Daniel Tobjörk.

(II) The author was responsible for sample preparation, analysis of results and writing the first draft. The inkjet-printing of electrodes was performed by A. Määttänen, AFM analysis was carried out by P. Ihalainen, TEM images were taken by M. Keppeler, screen printing was performed by D. Valtakari and spray coating was carried out by J. Hassinen.

(III) The author was responsible for sample preparation, analysis of results and writing the first draft. The inkjet-printing was executed by A. Määttänen, flexographic printing was performed by R. Bollström and AFM analysis was carried out by P. Ihalainen.

(IV) The author was responsible for sample preparation, analysis of results and writing the first draft. The inkjet-printing was executed by A. Määttänen, TEM images were taken by M. Keppeler and AFM analysis was carried out by P. Ihalainen.

(V) The author was responsible for sample preparation, analysis of results and writing the first draft. The inkjet-printing was performed by A. Määttänen, stability studies of the sensor were carried out by J. Koskela and optical microscopy images were taken by T. Gulin.

(VI) The author was responsible for sample preparation, analysis of results and writing the first draft. The inkjet-printing was performed by A. Määttänen and gold nanoparticles were synthesized by B. Torngren.

(VII) The sensing ink was prepared and printed by the author. The author was also responsible for writing part of the first draft.

LIST OF SUPPORTING PUBLICATIONS

SI R. Bollström, D. Tobjörk, P. Dolietis, T. Remonen, C. Wikman, S. Viljanen, **J. Sarfraz**, P. Salminen, M. Lindén, C. Wilén, J. Bobacka, R. Österbacka, M. Toivakka. **Roll-to-roll printed electronics on paper**. Papercon Conference. (2012).

SII P. Ihalainen, H. Majumdar, T. Viitala, B. Törngren, T. Närjeoja, A. Määttänen, **J. Sarfraz**, H. Härmä, M. Yliperttula, R. Österbacka, J. Peltonen. **Application of Paper-Supported Printed Gold Electrodes for Impedimetric Immunosensor Development**. Biosensors, 3 (2013) 1 - 17.

SIII V. Leminen, M. Kainusalmi, P. Tanninen, H. Lindell, J. Varis, S. Ovaska, K. Backfolk, M. Pitkänen, T. Sipiläinen-Malm, J. Hartman, E. Rusko, L. Hakola, P. Ihalainen, A. Määttänen, **J. Sarfraz**, J. Peltonen. **Aspects on Packaging Safety and Biomaterials**. 26th IAPRI Symposium on Packaging (2013) 483 - 493.

SIV P. Ihalainen, A. Määttänen, M. Pesonen, P. Sjöberg, **J. Sarfraz**, R. Österbacka and J. Peltonen. **Paper-supported nanostructured ultrathin gold film electrodes - characterization and functionalization**. Applied Surface Science, 329 (2015) 321 - 329.

SV V. Leminen, M. Kainusalmi, P. Tanninen, H. Lindell, J. Varis, S. Ovaska, K. Backfolk, K. Mielonen, M. Pitkänen, T. Sipiläinen-Malm, E. Rusko, L. Hakola, **J. Sarfraz**, P. Ihalainen, J. Peltonen. **Ways for Improving the Safety of Fibre-based Food Packages,** 27th IAPRI Symposium on Packaging. (2015) 249 - 266.

1. INTRODUCTION AND OUTLINE

Many gases like ammonia (NH_3), carbon monoxide (CO), nitrogen oxide (NO) and hydrogen sulfide (H_2S) are toxic and pose threat to humans and animals. Exposure to gaseous ammonia at concentrations of 50 - 100 parts per million (ppm)[1] can cause severe burns to the skin, eyes, throat and lungs. In the case of exposure at or above 5000 ppm, blindness, lung damage and death are possible. Even at low concentrations, ammonia exposure causes coughing and irritation. Persons with asthmatic conditions are particularly prone to these effects.[2] At concentration levels of 25 ppm, chronic exposure can lead to damage of the eyes, liver, kidneys and lungs.[3]

CO is a byproduct of incomplete combustion reactions. Exposure at concentrations of 30 ppm can result in the weakening of heart contractions, reduction in ability to perform manual tasks, and general drowsiness.[4]At concentrations greater than 35 ppm for extended durations (>24 hours), carbon monoxide exposure can result in headache, irritability, blurred vision, lack of coordination, nausea, dizziness, and death. According to United States government regulations, the threshold level value for CO is 50 ppm for an eight hour exposure.[5]

NO at 1 - 5 ppm, is a general irritant of the respiratory system as well as the eyes. Exposure over time results in fluid build-up in the lungs, nausea, and fatigue. Higher concentration exposures cause swelling of the throat, reduced oxygenation in the blood, and in severe cases death.[6]

H_2S gas is also of particular interest because of its toxicity. The threat to humans and animals by H_2S gas is the primary motivation for the development of a low-cost H_2S gas sensor. H_2S is a very poisonous and flammable gas and has a characteristic rotten egg smell.[7] However, because of temporary paralysis of olfactory nerves at concentrations higher than 100 ppm, the smelling capability is severely compromised. H_2S gas is commonly known as sewer gas, stink damp, swamp gas, and manure gas.[8] It is generated by the bacterial degradation of organic matter in the absence of oxygen, during volcanic eruptions, extraction of natural gas or oil, mining activity, refining of natural gas and crude oil, etc.[9] Exposure to low concentrations of H_2S can result in eye irritation, a sore throat and cough, shortness of breath, and fluid retention in the lungs. These symptoms usually disappear in a few weeks. Long-term, low-level exposure may result in fatigue, loss of appetite, headache, irritability, poor memory and dizziness. Higher concentrations, i.e. 700 - 800 ppm tend to be fatal.[10] H_2S sensors are important for environmental monitoring and for industries including food packaging, mining, defense, oil and gas.[11-16] The common sensor types employed for H_2S sensing include semiconducting metal oxide sensors, electrochemical sensors, optical sensors, conducting polymer based sensors, piezoelectric sensors and chemiresistive sensors.

In general a gas sensor is a device which transduces the chemical information resulting from the receptor-analyte interaction into a physical signal like change in mass, resistance or temperature. An ideal gas sensor should be selective, sensitive, reversible, durable, easy to manufacture and easy to calibrate and use.

Transducers are sometimes used as a synonym for sensors. A transducer is a device which converts a stimulus in to any other form. Jocob Fraden in the handbook of modern sensors has defined that "a sensor is a device that receives a signal or stimulus and responds with an electrical signal."[17] According to this definition a sensor is a device which converts a physical, chemical or biological signal into an electrical signal. Therefore we can say that a sensor is a type of a transducer in which the output signal is limited to electrical signal. Sensors typically mimic human senses, e.g. in human olfactory system the output is also an electrical signal which is transmitted to the nervous system.

In the human olfaction (sense of smell) the presence of gaseous compounds can sometimes be perceived by smell. The human olfactory system is responsible for the recognition of odours and it can classify at least ten primary qualities.[18] The human olfactory system is shown in detail in Figure 1 and Figure 2. The olfactory epithelium and olfactory bulb are shown in Figure 1. The nasal cavity that detects smell is beneath the eyes and is lined with a sticky mucus fluid (Figure 2). The smell molecules have to pass through mucus membrane in order to interact with the receptors. Binding proteins located in the mucus membrane bind the smell molecules. Specialized olfactory nerve cells are another important part of the olfactory system. The olfactory nerve cells are formed by three main parts: the cell body in the middle, on one end tiny hairs called cilia and on the other end nerve extensions called axons (Figure 2). The odour molecule in mucus membrane specifically interacts with the receptors on the hair like cilia of olfactory nerve cells and generates a potential that is transmitted, by the cell axon, to the secondary neurons, in the glomerula of the olfactory bulb.[18] The Axons transport the signal by forming a bundle in order to reach the olfactory bulb and as a group pass through a porous ultra-thin piece of bone called cribriform plate. In olfaction the selectivity between different molecules is achieved by the generation of different potential signals in different types of receptor cells. When the receptor cells interact with a given molecule they create a characteristic pattern which makes it possible to identify that particular molecule. The information transmitted by the olfactory nerve cells is processed in the brain that generates the odour sense. In man, the olfactory epithelium is restricted to an area of about 2.5 cm^2 in each nasal mucosa.[19] The olfactory sensing system is highly sensitive and selective with a detection threshold that can be as high as one part of an odorant substance in 10^{12} parts.[20]

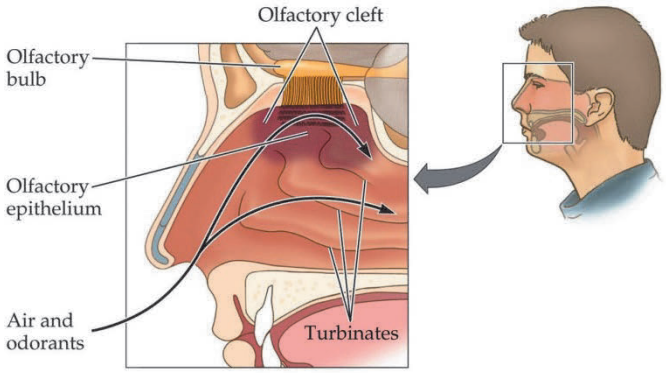

Figure 1. An illustration of the position of the olfactory epithelium and air flow during normal breathing. 21

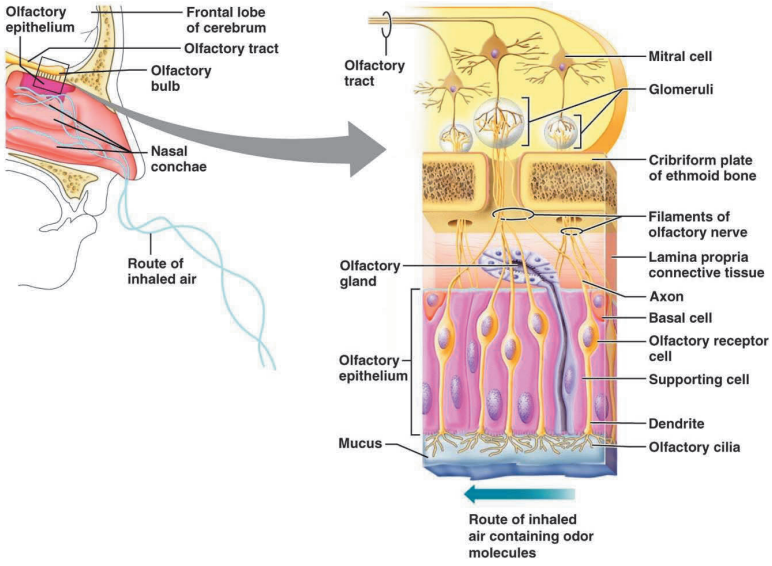

Figure 2. Details of the olfactory epithelium and olfactory bulb section.[22]

The odour properties, including perceived intensity of a molecule depend on the shape, size and the characteristics of the polar group, so that low volatility species can be sensed intensely, while another present in high concentration can have only a low intensity smell.[23] Furthermore the olfaction is subject to variation with health, diet or age and cannot be used for accurate quantitative or qualitative detection of analytes.

In this thesis chemiresistive type H_2S gas sensors have been developed, characterized and demonstrated. In paper I drop-casted deprotonated emeraldine base (EB) (poly)aniline (PANI) - copper chloride films on paper substrates containing inkjet-printed silver electrodes were prepared and were shown to be promising low-cost H_2S gas-sensors at room temperature. These films showed large changes in the conductivity

($>10^3$) upon exposure to low concentrations of H_2S (10 ppm) due to the formation of CuS and concurrent protonation of PANI.

In paper II, the use of printing techniques was extended to the fabrication of the sensing film in a H_2S sensor. The sensor was based on an aqueous PANI-metal salt ($CuCl_2$) composite. The sensing film was produced by screen printing and spray coating the sensing material on interdigitated silver electrodes. The electrodes were inkjet-printed on a paper substrate. The H_2S sensing functionality with respect to pH, PANI and metal salt concentration was optimized. In addition, the long term stability and humidity effects on the sensor performance were investigated. The printed chemiresistors showed more than five orders of magnitude change in resistance within 20 min of exposure of 15 ppm H_2S at room temperature.

In paper III a stable dispersion was developed which was suitable for roll-to-roll printing of a film exhibiting H_2S gas sensing functionality. The dispersions were made from copper chloride (CC) in combination with either citric acid (CA) or CA and PANI. In paper III, a mixture of CC and CA was optimized for printability as well as for sensitivity towards H_2S gas. Furthermore the stability of an aqueous PANI dispersion was studied after the addition of CC or a CC-CA mixture as a function of pH. The stable dispersions were printed on top of flexographically printed interdigitated silver electrodes and their sensitivity towards 10 ppm H_2S was verified by following the change in resistance.

In paper IV fully printed copper acetate based H_2S sensors on paper substrate was presented. The sensors showed several orders of magnitude change in resistance ($>10^8$) when exposed to 10 ppm of H_2S gas at room temperature. The effect of different solvents, film thickness and substrates (absorbing and nonabsorbing) were studied to optimize the sensor response. The large resistance changes were associated with the difference in resistivity between the metal salt and the resulting metal sulfide.

In paper V the performance of a printed copper acetate based H_2S sensor with irreversible electro-optical response was investigated. The sensitivity, long term stability, humidity effects, cross-sensitivity and selectivity of the H_2S sensor were studied. The sensor can be utilized for quantitative detection of H_2S. Furthermore, a simple optical indicator based on copper acetate for H_2S sensing was also presented. The indicator was calibrated using grayscale images for different concentrations of H_2S.

In paper VI the improvement of the sensitivity of the copper acetate based H_2S sensor down to sub-ppm level of H_2S was demonstrated by incorporation of catalytic gold nanoparticles (AuNPs) and surface plasma treatment.

In paper VII a demonstration of wireless detection of biogenic H_2S produced by the degradation of poultry meat using a copper acetate based H_2S sensor is shown.

2. AIMS OF THE STUDY

H_2S gas is a toxic gas and poses threat to human health. It can be lethal if inhaled in high concentrations. Therefore the monitoring and control of H_2S level is of great interest for a wide range of application areas including food quality control, defense and anti-terrorist applications and air quality monitoring in e.g. mines.

The overall aim of this study was to develop a low cost H_2S gas sensor on a flexible substrate. The performance of the sensor would include high sensitivity and selectivity, short response time and low detection limit. One important objective was also to verify the performance of the sensor in an application under real circumstances.

Development of a printable ink formulation of the gas-sensing material was one of the most essential specific aims. Printability is important since it enables, through solution processability, the mass production of the sensors and lowers the unit cost. The printable functional inks were developed by optimizing the printing parameters like surface tension, viscosity and particle size.

One specific goal was to improve the detection limit of the sensor down to sub-ppm level. The hypothesis for reaching this goal was to use catalytically active metal nano-particles and subsequent plasma treatment of the sensing film.

3. BACKGROUND AND LITERATURE REVIEW

3.1. Types of gas sensors

The gas sensors can be categorized according to the reception and transduction principles. The most common types of gas sensors are discussed here.

3.1.1. Electrochemical sensors

Electrochemical gas sensors react with the target gas and produce an electrical signal which is proportional to gas concentration. Electrochemical sensors can be broadly divided into amperometric, potentiometric and chemiresistive sensors based on their working principle.

3.1.1.1. Potentiometric sensors

Potentiometric sensors ideally operate at zero current and measure the potential difference or electromotive force (EMF) between the sensing or working electrode and the reference electrode. Potentiometric gas sensors are most commonly used for the detection of oxygen. In a typical oxygen lambda sensor which is used in automobiles, two electrodes are deposited on the two sides of an oxygen ion conducting solid electrolyte (zirconium dioxide). One of the electrodes which are in contact with the known oxygen partial pressure is called the reference electrode while the other electrode which is in contact with the unknown oxygen partial pressure is the working electrode as shown in Figure 3. The difference in concentration of oxygen molecules in the exhaust gas and the ambient air drives the oxygen ions from higher to lower concentration. When the electrodes are in contact with two different oxygen partial pressures and isolated from each other, an EMF is developed due to the movement of oxygen ions from one platinum layer to the other.[24] The EMF is described by the Nernst equation as shown in equation (1).

$$E = \frac{RT}{zF} \ln \frac{P_t}{P_w} \quad (1)$$

Where

- P_t is the partial pressure of oxygen at the reference electrode
- P_w is the partial pressure at the working electrode
- R is the gas constant
- T is the temperature in Kelvin
- z is the number of electrons taking part in the reaction
- F is the Faraday's constant.

These sensors usually operate at ≥ 300°C. The schematic illustration of a potentiometric oxygen lambda sensor is shown in Figure 3. Liang et al.[25] showed a potentiometric sensor based on a sodium super ionic conductor and a Pr_6O_{11}-doped SnO_2 sensing electrode for the detection of H_2S.

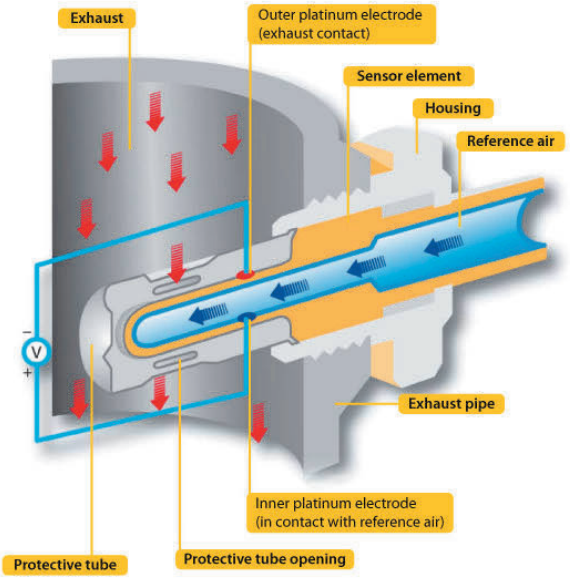

Figure 3. The principle of an oxygen lambda sensor. [26]

3.1.1.2. Amperometric sensors

In amperometric sensors fixed (occasionally variable) potential is applied, which induces the oxidation or reduction reaction of the analyte molecules at the working electrode. The current is generated due to this reaction which is related to the analyte concentration.

In the simplest scheme an amperometric sensor consists of two electrodes, a working electrode and a counter (sometimes called auxiliary) electrode. However, most amperometric sensors have a third reference electrode which assists to maintain a constant voltage at the working electrode. In an electrochemical cell a solid or liquid electrolyte is used to allow the transportation of ions between the electrodes. Typically a gas permeable membrane covers the inlet of the sensing electrode which provides selectivity and helps to limit diffusion such that it becomes the rate determining step. The membrane also serves to prevent leakage or drying out of the electrolyte.[27] The reaction rate, reflected by the current at the sensing electrode, can be limited by the rate of reaction at the surface or the rate of diffusion of the analyte gas to the electrode surface. If operated under diffusion-limited conditions, the current is proportional to the concentration of the analyte in the surrounding gas.[28] Faraday's law relates the

observed current (sensor signal) to the number of reacting molecules as shown in equation (2).[29]

$$I = n \times F \times Q \times C \quad (2)$$

- I = current in coulombs/s
- Q = the rate of gas consumption in m^3/s
- C = the concentration of analyte in mol/m^3
- F = Faraday's constant (9.648×10^4 coulombs/mol)
- n = the number of electrons per molecule participating in the reaction.

Figure 4 shows a schematic diagram of an amperometric sensor with a three-electrode configuration. The electrochemical cell consists of a working electrode, a counter electrode and a reference electrode connected with a potentiostat, a gas permeable membrane and the electrolyte.

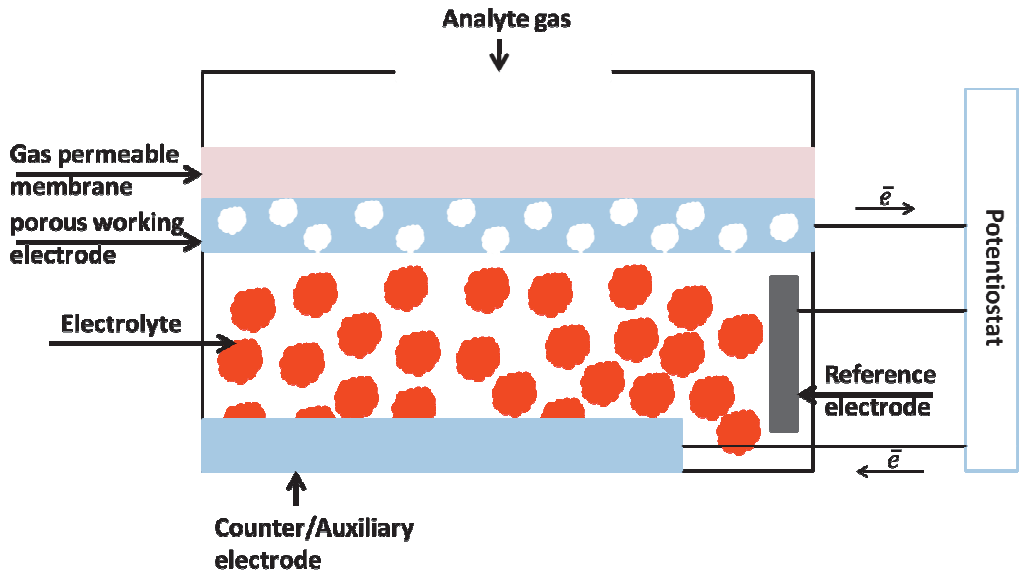

Figure 4. A schematic diagram of an amperometric sensor with a three-electrode configuration.

One of the main differences between potentiometric and amperometric sensors is that the sensing principle in a potentiometric sensor is thermodynamic, i.e., it assumes that all reactions relating to the sensing (chemical and diffusion) processes are at equilibrium. While the amperometric sensors rely on Faraday's law and a dynamic reaction achieving a steady-state condition in the sensor. This implies that the amperometric sensor signal is dependent on the size of the electrode and the rate of analyte reacting at the electrode surface, while the potentiometric sensor assumes a thermodynamic potential independent of the size of the electrode.[28] Table 1 lists electrochemical reactions for aqueous electrolyte amperometric gas sensors.

Table 1. Electrode reactions for aqueous electrolyte amperometric gas sensors.[28]

Target gas	Electrode reaction
H_2	$H_2 + 2OH^- = 2H_2O + 2e^-$
CO	$CO + H_2O = CO_2 + 2H^+ + 2e^-$
O_2	$O_2 + 4H^+ + 4e^- = 2H_2O$
NO_2	$NO_2 + 2H^+ + 2e^- = NO + H_2O$
NO	$NO + 2H_2O = NO_3^{2-} + 4H^+ + 3e^-$
H_2S	$H_2S + 4H_2O = SO4^{2-} + 10H^+ + 8e^-$
SO_2	$SO_2 + 2H_2O = SO_4^{2-} + 4H^+ + 2e^-$

Typically in an amperometric H_2S gas sensor a solid polymer electrolyte coated electrode is used for quantitative determination of gas-phase H_2S.[30]

3.1.1.3. Chemiresistive sensors

A simple chemiresistive gas sensor consists of a gas sensitive film deposited on top of the interdigitated electrodes. Upon interaction of the film with the analyte gas the conductivity of the film changes which can be related to the concentration of the analyte gas. Semiconducting metal oxides such as SnO_2, WO_3, TiO_2 etc. as well as polymer composites are commonly used as gas sensitive materials for sensing CO_2, H_2S, NH_3, O_3, NO_X etc.

Semiconducting metal-oxide sensors

Semiconducting metal oxide thick and thin films are employed for H_2S gas sensing because of their low cost, simple construction, small size and low power consumption. These sensors typically operate at temperatures between 200 - 500 °C.[31] With the interaction of the analyte gas with the metal oxide film, the electronic properties of the film change, resulting in the change in resistance of the film.[32] There are two types of metal oxide sensors; n - type (zinc oxide, tin oxide, titanium oxide, or iron (III) oxide) and p - type (nickle oxide, cobalt oxide).[33]

The n - type metal oxide films are mostly sensitive towards reducing gases. Oxygen in the air reacts with the n - type metal oxide surface and traps any free electrons on the surface or at the grain boundaries resulting in an increase of resistance of the film. When these films are exposed to the reducing gas like H_2, CH_4, CO, C_2H_5 or H_2S the resistance drops because of the release of electrons due to the interaction between the reducing gas and oxygen.[34] The sensitivity of the metal oxide film is affected by the film thickness and the operating temperature with thinner films being more sensitive.[35] The sensitivity can be improved by the addition of a catalytic metal to the oxide film.[36] Normally the change in conductivity and/or impedance is measured for semiconducting metal-oxide based sensors. The common metal oxides employed for sensing H_2S gas are SnO_2, Fe_2O_3, WO_3, $BaTiO_3$, ZnO and In_2O_3.

Use of catalyst particles

Noble metals have been used for enhancing the performance of gas sensors by utilizing their catalytic ability for superior oxygen dissociation.[37] Metals that have been used for doping the sensing material include e.g. Pt, Au, Pd and Ag.[38, 39, 40] These metals can act as adsorption-desorption sites for catalyzing the reaction between the sensing material and the analyte molecules. Furthermore the use of these metals can significantly enhance the ionosorption of oxygen on the sensing material. This ionosorption can be further increased for example by oxygen plasma treatment. [34] There are also reports which indicate that the plasma treatment can decrease the operating temperature of the metal oxide based sensors from initially high temperatures down to room temperature.[41, 42]

Conducting polymer based sensors

Conducting polymer composites consist of conducting particles such as polypyrrole, carbon black and carbon nanotubes interspersed in an insulating polymer matrix.[34] When the concentration of conducting material exceeds the percolation threshold, a percolated conducting path is formed in the polymer matrix which results in the increase of conductivity. When the analyte gas interacts with the composite material the percolated conducting path collapses due to the swelling of the polymer resulting in an increase of resistance of the polymer composite.

Metal salts of polyaniline composites have been reported to have superior sensitivity towards H_2S gas. The change in resistance of the sensing film upon exposure to H_2S gas was explained by the formation of metal sulfide and subsequent protonation of polyaniline.[43] A polyaniline nanowire-gold-nanoparticle hybrid network was reported to show improved sensitivity towards H_2S.[44] Polymer composite based sensors typically operate at room temperature. The main disadvantage of these sensors is their high sensitivity towards humidity.

3.1.2. Optical sensors

Optical sensors commonly transduce analyte information to an optical signal.[45] Typically optical sensors consist of a wave guide (or optical fiber) and a coating. The analyte interacts with the sensitive coating and the qualitative or quantitative information about the analyte can be obtained due to the absorption or emission phenomenon. Generally optical sensors can be further categorized into direct and reagent mediated sensors. In direct sensing, the analyte is detected directly via its intrinsic optical property (e.g., absorption or luminescence). For reagent-mediated sensors, a change in the optical response of an intermediate agent (e.g., an analyte-sensitive dye molecule) is measured.[46]

3.1.3. Piezoelectric sensors

Piezoelectric sensors can be further categorized into Quartz-crystal microbalance (QCM) sensors[47, 48] and surface acoustic wave (SAW) sensors.[49, 50] Both QCM and SAW devices transduce the sensor response into a change of mass signal. In operation mode, the device resonates at a characteristic frequency via excitation by a specific oscillator. When the analyte gas is adsorbed, the mass of the device increases resulting in a decrease of the resonating frequency. SAW devices are based on the principle that a Rayleigh wave travels over the surface of the device instead of its volume. SAW sensors can operate at much higher frequencies than QCM sensors. QCM devices can typically detect 1 ng of mass change while SAW devices can detect down to 1 pg of mass change.[46]

A gold piezoelectric quartz crystal coated with tetramethylammonium fluoride tetrahydrate has been used to detect H_2S gas with a center frequency of 9 MHz.[51] A SAW device for H_2S gas sensing has been reported with the active film consisting of WO_3 on $LiNbO_3$.[52]

3.1.4. Capacitive gas sensors

A capacitive gas sensor is based on a capacitance change. The capacitance can be expressed in terms of permittivity, area and distance between the electrodes according to equation (3).

$$C = \frac{A \varepsilon_0 \varepsilon_r}{d} \tag{3}$$

- C is the capacitance
- ε_0 is the permittivity of vacuum
- ε_r is the relative permittivity
- A is the area of the electrodes
- d is the distance between the electrodes also known as the thickness of the dielectric

Capacitive detection is based on a change in ε_r, d or A induced by adsorbed gas molecules. The changes in the permittivity of the dielectric due to the interaction between an immobilized antibody and antigen on an electrode can be used to detect bio-molecules.[53] The most common capacitance sensor is a humidity sensor. Water has a large dielectric constant, upon adsorption of water molecules the capacitance of the sensor changes due to the change in the permittivity of the dielectric. Also ammonia (NH_3) has been detected by a capacitive sensor,[54] but this method is not so well applicable for, e.g., methane (CH_4).[55]

3.1.5. Catalytic gas sensors

Catalytic sensors have been used for the detection of combustible gases. The first catalytic sensor was developed in 1923 by Jones[56, 57] for the detection of methane. These sensors catalytically reduce the ignition temperature of the combustible gases and can be further divided into pellistor - type and thermoelectric type sensors.

A pellistor - type gas sensor as shown in Figure 5 consists of two platinum coils. These coils serve as a heater as well as a thermometer and are further connected to an active and inactive bead. The active bead is activated by a catalyst while the inactive bead has no catalyst. Upon application of voltage, the circuit heats up the coils and the temperature of the beads are raised which causes the ignition of the analyte gas at the detector coil. Upon ignition the temperature further rises which causes an imbalance in the voltage of the wheatstone bridge which creates the sensor signal.

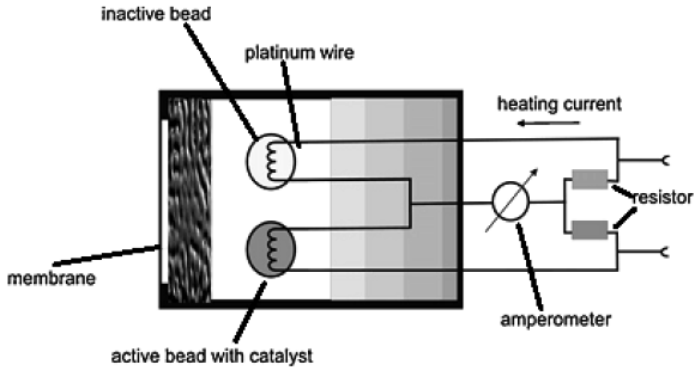

Figure 5. A pellistor-type gas sensor [27]

The first thermoelectric gas sensor was developed for hydrogen gas detection in 1985 by McAleer.[58, 59] When a thermoelectric gas sensor is exposed to hydrogen gas, catalytic exothermal oxidation reaction takes place which produces an electrical signal that enables the detection of hydrogen gas. Thermoelectric gas sensors use the thermoelectric effect to generate the electric signal. The thermoelectric effect or more specifically the Seebeck effect occurs as a result of a temperature difference between two points of a conductor or semiconductor material which gives rise to a voltage difference between these points.[24]

3.2. Gas sensor performance

The gas sensor performance can be judged based on the following parameters.

3.2.1. Sensitivity

Sensitivity of a gas sensor can be defined as the ability of the sensor to detect small concentrations of gas molecules. Generally sensitivity is measured as the slope of the response curve. The response curve is normally a plot between the sensor response and the concentration of the gas. Sensitivity can also be reported as a normalized ratio of the response signal over the base line. This method often referred to as $R\text{-}R_o$ or $\Delta R/R_o$, is the standard for reporting the performance of chemiresistive type gas sensors where R_o and R are the initial and final resistance values. In Figure 6 a typical sigmoid shape response curve of a gas sensor is presented. Figure 7 illustrates the difference in sensitivity of two gas sensors.

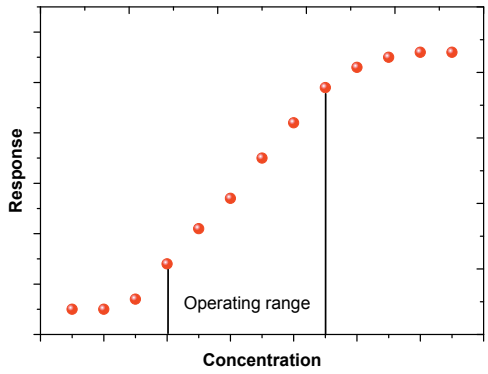

Figure 6. A typical sigmoid shape response curve of a gas sensor and illustration of the linear operating range.

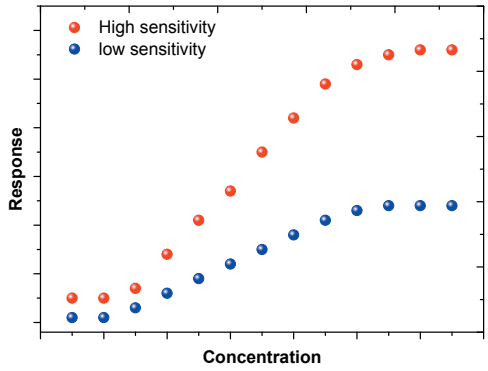

Figure 7. An illustrative plot of high and low sensitivity.

3.2.2. Selectivity

The selectivity of a gas sensor can be defined as an ability to distinguish between gases. Selectivity is generally associated with the false positive probability. In medical

applications selectivity is referred to as specificity. Examples of excellent and poor selectivity for an array of four sensors are described in Table 2.

Table 2. Examples of A) excellent and B) poor selectivity for an array of four sensors with positive response indicated as + and no response indicated as —.

A	NH_3	CO	NO	H_2S	B	NH_3	CO	NO	H_2S
Sensor1	+	—	—	—	Sensor1	+	—	+	—
Sensor2	—	+	—	—	Sensor2	+	+	+	+
Sensor3	—	—	+	—	Sensor3	—	+	+	—
Sensor4	—	—	—	+	Sensor4	—	—	+	+

3.2.3. Lower limit of detection (LOD)

The lower limit of detection of a gas sensor can be defined as the minimum concentration of the analyte which can be detected by the gas sensor. The lower limit of detection is a statistically significant point where one can clearly differentiate between the response of the device from the background noise.

3.2.4. Response time and onset time of detection

The response time of a sensor is defined as the time to reach 90% of the steady state value excluding the onset time of detection and the onset time of detection can be defined as the time that it takes for the sensor to respond to the presence of the analyte.[60] Figure 8 describes the response time and onset time of detection of a given sensor.

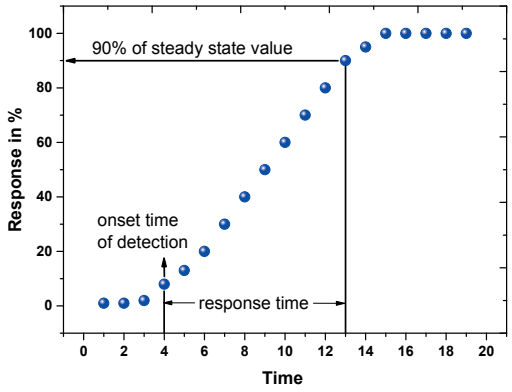

Figure 8. Illustration of the response time and onset time of detection.

3.2.5. Coefficient of variation (CV)

The coefficient of variation is the measure of reproducibility of the sensing device's response at a given operating point and can be defined as a ratio between the standard

deviation (S) and mean value ($\bar{x}$). It is often expressed as a ratio and sometimes multiplied with 100 to get a percentage.

3.3. Colloidal dispersions

A colloid is a system where one phase is dispersed in another phase. If the dispersion medium or continuous phase is gas the colloidal system is called an aerosol. When solid colloidal particles are dispersed in a liquid medium the colloidal system is called a sol or a hydrosol (when the medium is water). Particles (the dispersed phase) are classified as colloidal particles when at least one dimension of the particles lies between 1 nanometer and 1 micrometer. The liquid-in-liquid colloidal systems are called emulsions and gas-in-liquid systems are referred to as foams.

As colloidal particles have very small size, they consequently have a very large interfacial area in the dispersion medium. The properties of colloids depend very much upon the properties of this interface.[61]

3.3.1. Dispersion properties

Dispersions of colloidal particles in aqueous solutions at high solids concentrations are very important in different industrial processes, such as ceramic processing, printing, cosmetics etc. Mechanical strength, elastic and flow behaviour, rate of settling and surface wetting properties are common dispersion properties which are determined by the interaction between the particles. These properties can be adjusted by electrolytes, polymers, surfactants and by adjusting the pH.

3.3.1.1. Surface charge

When a surface is immersed in liquid, it can acquire charges in a number of ways. One of the mechanisms is the adsorption of ions from a solution on an initially uncharged surface. Another possible mechanism is the ionization or dissociation of surface groups.

When nanoparticles are brought into contact with polar medium most of the surfaces of the particles acquire charge due to:

- Ionization (depending upon pH like protonation/deprotonation of surface groups)
- Ion adsorption (due to unequal adsorption of ions charge appears on the surface)
- Ion dissolution (due to unequal dissolution of ions charge can appear)

The surface charge of an oxide is the result of acid-base equilibrium. It is a function of both pH and ionic strength as described in Figure 9.

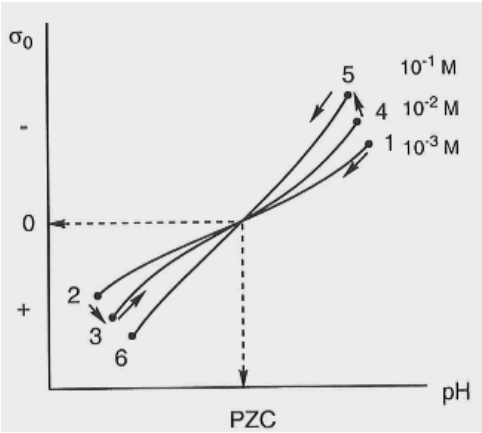

Figure 9. Proton titration curves of an oxide suspension for various electrolyte concentrations. [62]

The surface may be positively or negatively charged, or it may carry no net charge (at point of zero charge, PZC).Several factors influence the PZC such as

- The polarization of surface groups (related to the size and charge of the particles).
- The crystallinity, as the coordination number is not necessarily the same in different crystal forms.
- Previous treatments on the particles, for instance heat treatment will strongly affect the surface concentration of hydroxyl group.[63]

3.3.1.2. Point of zero charge (PZC)

The PZC is the pH at which the positive and negative charges of a zwitterionic surface are balanced. Respectively, it can be defined as the pH at which the surface charge density is neutralized to zero. The PZC has also been found to be the point of minimum solubility, since the chargeless surface is then at its most in a hydrophobic state.[61] The surface charge density can be defined in terms of surface concentrations of OH^- and H^+ as shown in equation (4).

$$\sigma_o = F\,(\Gamma_H - \Gamma_{OH}) \qquad (4)$$

- σ_o is the surface charge density
- F is the Faraday constant
- Γ_H is the adsorption density of H^+
- Γ_{OH} is the adsorption density of OH^-

PZC can be determined by acid base titration.[64]

3.3.1.3. Electric double layer (EDL)

When a substance is brought in contact with a polar medium, its surface gets charged. This charged surface influences the distribution of nearby ions in the polar medium. The ions which are oppositely charged to the surface (counter ion) are attracted towards the surface whereas co-ions (having the same charge as the surface) are repelled away from the surface. This together with a mixing tendency of thermal motion leads to a formation of an electric double layer made up of a charged surface and a neutralizing excess of counter ions over co-ions distributed in a diffuse manner in a polar medium.[65]

The most important factors that affect the stability of colloids are the polarizability through the Hamaker constant, the thickness of the diffuse layer in the EDL (the Debye thickness κ^{-1}) and the surface potential in the EDL. The overlapping EDL between two approaching colloidal particles leads in repulsive interactions which may be compensated for by attractive interactions. The overall total interaction is very important in the context of stability of a wide variety of colloidal systems, which range from food colloids, pharmaceutical dispersions and paints to colloidal contaminants in waste water.

In the structure of suspensions (sols) containing macromolecules such as polymers, polyelectrolytes (polymer molecules with charges) and proteins the electrostatic forces play a vital role. In the case of polyelectrolytes and charged colloids the transport behavior such as rheology is also affected significantly by charge effects.[66]

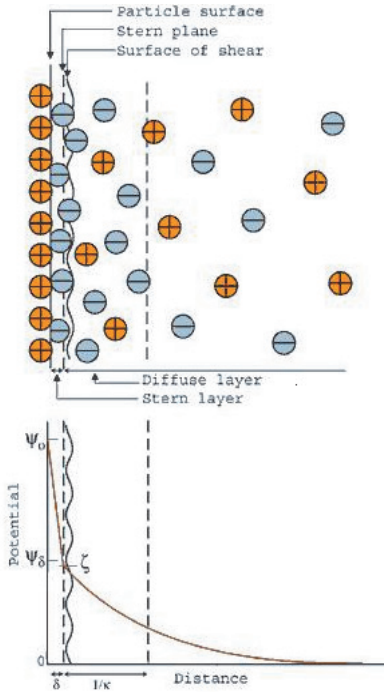

Figure 10. A schematic representation of the structure of the electric double layer according to the Stern model. [65]

3.3.1.4. Diffuse layer

When the surface of the particle is not charged, electrolyte, protons and counter ions are equally distributed in the surrounding liquid phase. When the particle surface is positively charged, there is a strong pull of attraction for negatively charged ions while the positively charged ions are repelled and vice versa. The ions adsorbed to the surface are located in the so called Stern layer (Stern plane), from which the potential decays exponentially towards the bulk liquid phase. This layer with decaying potential is called the diffuse layer, having a thickness called the Debye thickness, κ^{-1} (Figure 10).

3.3.1.5. Zeta potential ζ

The surface of shear is formed when the particle moves in a stationary liquid. The moving (kinetic) unit is formed by the particle and the liquid inside the shear plane. The potential in the shear plane is called the electrokinetic potential or the zeta potential, ζ. The surface of shear is often approximated to be located in the Stern plane.

Zeta potential gives an indication of the extent to which ions from the solution are absorbed into the Stern layer. When the solid surface is able to ionize (as with oxides) the ζ potential is a measure of the extent of ionization.[61] The most important factors that affect the zeta potential are pH and ionic strength.

3.3.1.6. Isoelectric point (IEP)

The IEP is defined as the pH at which the zeta potential is zero. It is determined by a pH titration (measuring the zeta potential as a function of pH). IEP is the same as PZC if there is no specific adsorption of ions onto the surface.

3.3.1.7. Interaction forces

There are several types of interaction forces between the colloidal particles. Among them the two forces, van der Waals force of attraction and charge related Coulombic forces form the basis of the classical DLVO theory which was proposed in 1940s by Derjaguin, Landau, Verwey and Overbeek.[61]

Van der Waals forces

The van der Waals forces are due to interactions between atoms and molecules. Depending upon the types of molecules van der Waals forces can be divided into three different categories.

(1) The Keesom forces which deal with two permanent dipoles. When two permanent dipoles come across each other, they have the ability to orientate in a way that the positive end of one dipole is attracted by the negative end of the other.

(2) The Debye forces which act between a freely moving permanent dipole and an induced dipole. The permanent dipole has the ability to induce and orientate a dipole in a polarizable molecule, atom or medium in such a way that it can be attracted.

(3) London dispersion forces which act between two induced dipoles. Due to fluctuations in the distribution of electric charge in a molecule or atom, a dipole is spontaneously induced and it induces other dipoles, which are then interacting. These forces may be attractive or repulsive and are always present as they do not require permanent dipoles.

Electrostatic forces

When two similarly charged particles approach each other, there is no Coulombic (electrostatic) interaction until their diffuse double layers are in contact. At this point, the ionic strength between the particles increases and the osmotic pressure which arises from the concentration difference between the particles pushes them apart. The repulsive force increases with decreasing distance. The main parameters which determine the repulsive forces are the surface (and hence the zeta) potential, which determines at which distance the repulsive interaction starts. The interaction depends on the size and shape of the particles, the distance between them, the surface potential, the ionic strength and the dielectric constant of the dispersing liquid.[61]

Born repulsion

These are very short range repulsive forces which arise from the mutual repulsion of electrons associated with the atoms of each particle.[61] These forces are normally not considered in stability theories.

3.3.2. DLVO Theory

The DLVO theory is of great importance because it deals with the stability of colloids. The theory deals with the overall potential energy of interaction, that is the result of all the attractive and repulsive forces either due to interaction of similarly charged double layers surrounding particles or due to Born repulsion. The overall potential energy of interaction is the sum of the attractive and repulsive potentials. When two particles approach, if the energy increases, it means that they experience a repulsive force, and if the energy decreases as the particles approach it means that they experience an attractive force.

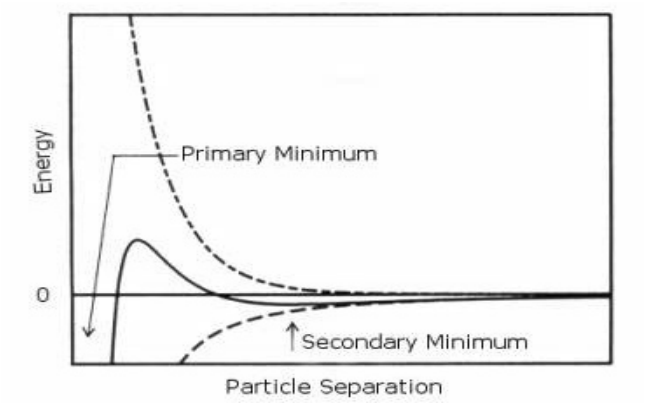

Figure 11. A graphical presentation of the DLVO theory. [67]

3.3.2.1. The primary and secondary minimum

When the particles are separated by relatively large distances, then the van der Waals attraction can be greater than the double layer repulsion giving rise to a secondary minimum as shown in Figure 11. In such situation particles may aggregate with a relatively large distance between them, a process called flocculation. Since the secondary minimum is quite shallow, flocculation of this type is easily reversible, and particles can be separated by agitation or even by Brownian motion.[61] Aggregation related to the primary minimum involves much shorter inter-particle distances. These so called coagulated structures are too strong to be degraded by Brownian motion or light agitation.

3.3.2.2. Effect of radius of particle

Both attractive and repulsive potential energies are directly or indirectly affected by the particle radius. Thus for a particular set of conditions the energy barrier to coagulation is proportional to the radius.

3.3.2.3. Effect of electrolyte concentration

With the increase of electrolyte concentration, the thickness of the double layer decreases which means that the energy barrier to coagulation decreases or disappears through weakened repulsion. Sufficiently high ionic strength favors coagulation.

Furthermore the decrease of the height of the energy barrier also depends on the charge number of the added ions of opposite charge. Trivalent ions are more effective than divalent ions which in turn are more effective than monovalent ions in influencing the critical coagulation concentration. This effect is known as the Schulze-Hardy rule.

3.3.2.4. Effect of surface potential

Generally the addition of electrolyte would tend to lower surface potential and coagulation would then be expected at lower ionic strength.[61] Overall according to the DLVO theory the stability of a dispersion is increased by

- An increase in the particle radius
- An increase in the surface potential
- A decrease in the effective Hamaker constant
- A decrease in the ionic strength (increase in the Debye thickness) of the dispersing liquid
- A decrease in temperature

3.3.3. Steric stabilization

Steric stabilization may be achieved by adsorbing a polymer on the surface of the particle. The polymer projects loops and tails into the continuous phase and the interaction of these projections restrict the approach of particles to one another. Uncharged particles can be stabilized by this method. So in this case electric charge with its associated double layer is not necessary.

Often polymers used are block or graft copolymers (comprising of two or more homo polymer subunits linked by covalent bonds) consisting of hydrophilic segments and hydrophobic segments. The hydrophilic segments are adsorbed in aqueous phase, and the hydrophobic segments are adsorbed on the particle surface as shown in Figure 12.[61]

One of the examples is an Egyptian ink. Egyptian used hydrophilic polymers of biological origin which adsorb on the carbon particles. Although the particles by themselves are hydrophobic the adsorbed polymers provide them a hydrophilic coating. Examples of Steric stabilization are found in paints, food products, soils, ointments, pharmaceutical and many biological systems.[68]

It is interesting to note that colloids can, under certain conditions, also be destabilized by small amounts of polymer. This phenomenon is called flocculation through bridging, different from coagulation i.e. the destabilization by electrolytes.

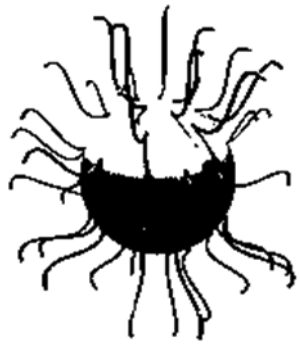

Figure 12. Steric stabilization through adsorbed polymers [69]

4. MATERIALS AND METHODS

4.1. Substrates

A multilayer coated paper substrate specially developed for printed electronics was used in this thesis. The multilayer coating was constructed to have a top layer for adjusting the printability properties and a bottom layer that provides excellent barrier properties against both organic and aqueous solvents.[70-72] The paper substrate was calendared three times (70 bar, 70 °C) in order to achieve a smooth surface with an average root-mean-square (RMS) roughness of 36 nm (5 µm x 5 µm AFM image).[73] Non-absorbing substrates polyethylene terephthalate (PET) and glass were also used in paper IV and VII.

4.2. Chemicals

4.2.1. Polyaniline

Since the discovery in 1977 that polyacetylene could be p- or n-doped to a metallic state[74, 75] a great deal of research and resources have been put in the development of new conducting polymers. Many new conducting polymers including polypyrrole, polythiophene, polyaniline etc. were developed. Polyaniline belongs to the class of conjugated polymers (alternating single and double bonds). It is one of the most studied conducting polymers because of its relatively high stability and wide range of conductivity.[76] Generally polyaniline can be found in one of the three oxidation states:

- Leucoemeraldine
- Emeraldine
- Pernigraniline

The equilibria between the different polyaniline states are shown in Figure 13.[77] Only emeraldine salt is the conducting state among the different forms of polyaniline. By protonation of emeraldine base through acid, an emeraldine salt can be obtained. Different states of polyaniline can be distinguished by their characteristic color. Leucoemeraldine has yellowish (sometimes colorless) color while emeraldine salt has green color and pernigraniline has dark blue color.

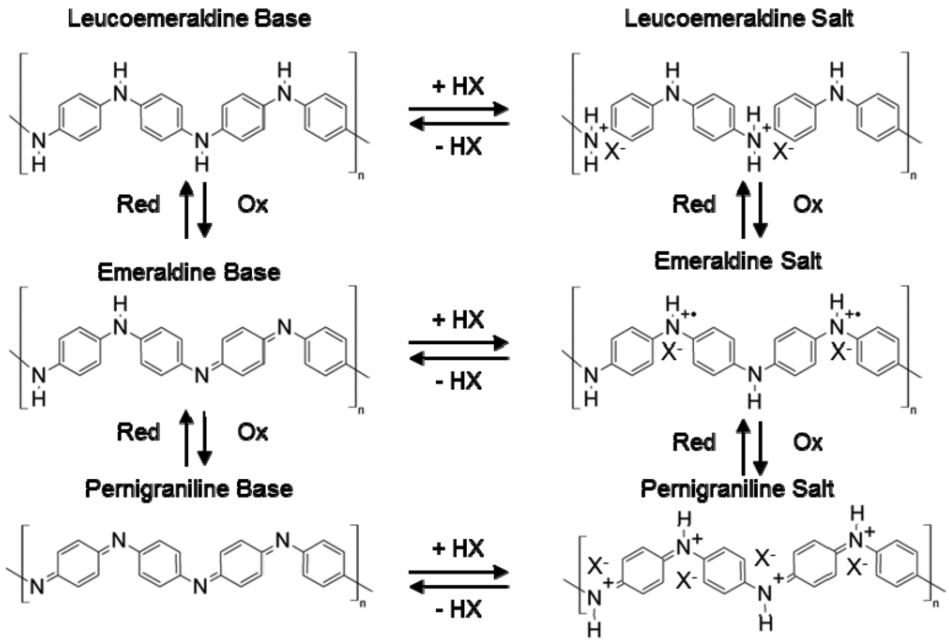

Figure 13 A schematic picture of the equilibria between the different polyaniline states.[77]

Polyaniline and polyaniline composites have been used in a number of applications including conductive adhesives, inks, paints, antistatic textiles, electrostatic discharge materials, electro-rheological materials, gas sensors, acid-base indicators, ion exchange materials, capacitors, energy storage devices, electromagnetic interference shielding, digital memory devices, artificial muscles, electrodes for rechargeable batteries, anode for microbial fuel cells, electro-chromic displays and smart windows, p–n heterojunctions, solar cells, diodes, organic or polymer light emitting diodes etc.[78, 79, 80]

A commercially available polyaniline emeraldine base powder and aqueous polyaniline emeraldine salt dispersion from Panipol Ltd. were used in this thesis.

4.2.2. Metal salts

Copper (ii) chloride (CC), citric acid (CA), and copper acetate (CuAc) from Sigma-Aldrich were used in this thesis.

4.2.3. Solvents

N-methyl-2-pyrrolidone from Sigma-Aldrich was used to dissolve polyaniline emeraldine base powder. Xylene from Sigma-Aldrich was used to disperse gold nano-particles for inkjet-printing. Iso-propanol and ethylene glycol from Sigma-Aldrich were used to tune the surface tension and viscosity of the aqueous solution of CuAc.

4.2.4. Functional inks

A commercially available silver nanoparticle-based ink (SunTronic U5603, Sun Chemicals) was used for inkjet-printing of interdigitated silver electrodes. The conductive silver (Ag) ink (product number: 125-06) was purchased from Creative Materials for flexographic printing of interdigitated silver electrodes.

Dodecanethiol-protected gold nanoparticles (AuNPs) were synthesized following the procedure reported by Hostetler et al.[81] The AuNPs (15 wt. %) were dispersed in xylene and inkjet-printed to produce interdigitated electrode structures on a paper substrate.[82, 83]

4.3. Printing and coating methods

4.3.1. Inkjet-printing

Inkjet-printing is a low cost non-contact printing technique that produces digital patterns at a relatively high resolution and with low material consumption.[84] It is widely used for printing of graphical documents. The interest in inkjet-printing of functional materials and functional devices has grown in recent years mostly because of low material consumption and the ease of changing the digital print patterns.[85, 86, 87] Inkjet-printing is a roll-to-roll compatible printing technique. The inks suitable for inkjet-printing have normally low viscosity (1-40 mPas), surface tension (25-35 mN/m^2) and particle size (less than 200 nm).

In this thesis Inkjet-printing was performed using a Dimatix Materials Printer (DMP-2831) with a cartridge that consisted of 16 nozzles.

4.3.2. Screen printing

Screen printing is mostly employed in batch printing and used for example for printing clothes, signs and irregularly formed items. In screen printing the ink is dragged across the surface of a screen and squeezed through the open pores of the patterned mesh onto the substrate.[88] Screen printing has been used in printing of functional devices such as antennas[89], photovoltaic cells[90], gas sensors[91] etc.

In this thesis screen printing was performed using TIC SCF-260B screen printer.

4.3.3. Flexography

Flexography is mostly utilized in printing of packages. In flexographic printing the ink is applied from the ink pan on the anilox roll by the help of a rotating rubber-covered fountain roller. The pattern to be printed is raised on a flexible plate that is attached to a cylinder. The raised surface of the printing roll are inked when in contact with an ink-

covered anilox cylinder that consists of homogeneously distributed, laser or mechanically engraved cells.[88] The ink is further transferred on the print substrate. A laser or mechanically engraved anilox roll is used for metering the ink amount. The thickness of the printed structure depends on the height of the cells of the anilox roll.[84, 88]

In this thesis the flexographic printing was performed by a custom built roll-to-roll hybrid printer.

4.3.4. Spray coating

Spray coating is a very simple coating method. The coating is prepared by spraying the solution/dispersion from an atomizer on the substrate. In this thesis the spray coating was performed by a custom made spray coater with a jetting frequency of 0.1 Hz The manufacturing and operation details of the spray coater have been discussed in detail by Salomäki et al.[92]

4.4. Characterization methods

4.4.1. Electrical characterization

A Keithley 2100 multimeter (two-probe setup) was used for electrical resistance measurements. A software 2100 KI-Link version 1.3 was used to follow the change in resistance as a function of time.

4.4.2. Surface characterization

X-ray photoelectron spectroscopy (XPS)

X-ray photoelectron spectroscopy is also known as electron spectroscopy for chemical analysis (ESCA). It is a highly surface sensitive technique for chemical analysis with sampling volume extending from the surface to a depth of approximately 5-10 nm.[93] In XPS the sample is irradiated with soft x-rays generated by bombarding a metallic anode with high-energy electrons. The energy of the X-rays is dependent on the used anode material, the typical ones being magnesium (Mg Kα, photon energy 1253.7 eV) and aluminum (Al Kα, photon energy 1486.6 eV) used under ultra-high vacuum conditions. Upon interaction of the photons with the sample, photoelectrons are emitted from the sample. The energy of these electrons is characteristic of the elements within the sampling volume. The number and kinetic energy of the emitted photoelectrons is detected and is converted into the binding energy (BE) by using equation (5).

$$BE = h\nu - \phi_s \quad (5)$$

Where hv is the energy of the incident x-rays and ϕ_s is the work function of the instrument i.e. the energy between the Fermi level and the vacuum level. The binding energy is characteristic for each element within the sampling volume but it is also influenced by the chemical environment of the atom. The information about chemical states of the elements can thus be obtained using XPS.[94]

The XPS measurements in this thesis were performed with a Physical Electronics Quantum 2000 scanning spectrometer using a monochromatic Al Kα x-ray source (1486.6 eV). An electron flood gun and a low energy ion gun were used for charge compensation. The detector position was at an angle of 45° in relation to the sample surface. The atomic concentration of the different elements was derived by calculating the area of the peaks and correcting for the sensitivity factors (using the software MultiPak v6.1A from Physical Electronics).

Grazing incidence X-ray diffraction (XRD)

The basic working principle of XRD is based on Bragg`s law according to equation (6).

$$n\lambda = 2d\sin\theta \tag{6}$$

Where λ is the wavelength of the incident X-ray, θ is the angle of incidence of the X-ray beam and d is the distance between the atomic layers in a crystal.

XRD is used to study crystalline materials. The faces of crystals reflect the X-rays at a certain angle of incidence according to Bragg's law. Constructive interference of these reflected waves creates a diffraction pattern. XRD can measure the average spacing between the layers or rows of atoms. It can determine the orientation of a single crystal. It can find the crystal structure of the unknown material and measure the size, shape, and internal stress of small crystalline regions. It can be used to measure the thickness of thin films and multi-layers and to determine the atomic arrangement. It can be applied to single and poly-crystals.

Grazing incidence diffraction (GID) mode is used to study thin films with a thickness range of 50-2000 nm. The incident angle theta in GID is from 0.2 to a few degrees. GID is employed to study the structural changes at the very surface of a sample. XRD was performed with a Bruker D8 Discovery (Bruker-AXS, Karlsruhe, Germany) using CuKα radiation (λ=1.54184 nm). For phase identification a PDF-2 database (2010) was used. The crystal sizes were calculated with the Topas 4.2 software (Bruker-AXS).

Transmission electron microscopy (TEM)

Transmission electron microscopy (TEM) is a high resolution characterization tool which can directly image atoms in crystalline samples down to 0.1 nm.[95] In TEM a stream of monochromatic electrons is produced with the help of an electron gun and condenser lenses. The condenser aperture is used to remove high angle electrons. The sample is placed between the condenser and the objective lenses. Only samples which

are thin enough to allow transmission of some electrons can be imaged with TEM. Heavy atoms having high electron density result in more interactions between the electrons in the primary beam and those in the sample, which in turn provides a higher contrast in the resulting image.[96] Electrons are detected both elastically and inelastically and are focused by different lenses before they reach the detection phosphor screen. TEM provides topological, morphological and compositional information about the sample.[97]

In this thesis the TEM images were taken using a FEI Tecnai F 20 instrument operating at 200 kV.

Atomic force microscopy (AFM)

Atomic force microscopy (AFM) can scan both soft and hard samples in ambient air or in a fluid environment and the sample surface can be imaged in its natural state. In AFM an image is created by scanning the surface using a physical probe and measuring the deflection of the cantilever due to interaction forces between the tip and the solid surface.

A typical AFM setup involves a sharp tip mounted on a micro-scale cantilever, a laser, a position sensitive detector, a xyz-piezoelectric tube (PZT) scanner, and control electronics. When the tip, with a radius of curvature on the nanometer scale, is brought near a sample surface, interaction forces (repulsive/attractive) between the tip and the sample lead to a deflection of the cantilever. The deflection is measured using a laser beam reflected from the top of the cantilever into an array of position sensitive photodiode.

In contact mode AFM, the cantilever deflection is usually kept constant during scanning by a feedback loop between the z-piezo and the photodiode. Hence any changes in cantilever deflection due to height differences on the sample surface are compensated by a corresponding change in the z-piezo position.[98]

In intermittent contact mode (also called as tapping mode AFM),[99] the cantilever oscillates with a pre-determined amplitude at or close to its resonance frequency. The oscillation is excited by a piezocrystal mounted in the cantilever holder. The tip is then brought close to the surface until it begins to lightly tap the surface during each oscillation cycle. The amplitude is altered when the tip is approaching the surface due to tip-sample interactions. The relative height position of the cantilever with respect to the sample is therefore adjusted to maintain a constant set-point amplitude during scanning, thus providing the feedback signal for topographical imaging.[98]

In this thesis an NTEGRA Prima AFM was used to analyze the topography of the paper substrate and the printed layers. Topographical imaging was carried out in intermittent contact mode. The Scanning Probe Image Processor (SPIP, Image Metrology, DK) software[100] was used for image and roughness analysis.

4.4.3. Dispersion characterization

Dispersion stability

Formulaction Turbiscan MA2000 was used to study the turbidity of the dispersions, providing a measure for the dispersion stability. The equipment works on the principle of multiple light scattering (MLS). MLS occurs when the analyzed colloidal dispersion is dense enough so that a light beam is scattered many times. The sample is irradiated with a light source and the ratio of the transmitted and incident light provides information about the instability like phase separation, sedimentation, creaming or particle aggregation (coalescence, flocculation).

Surface tension measurement

The surface tension was measured by a Du Noüy ring method and a maximum bubble pressure method. The Du Noüy ring method utilizes the interaction of a platinum ring with the surface being tested. The ring is submerged below the interface and subsequently raised upwards. When lifted through the surface the measured force will increase. The calculation of surface or interfacial tension by this technique is based on the measurement of this maximum force.

In the maximum bubble pressure method an inert process gas (nitrogen or dry air) is bubbled slowly through two probes of different radii (r1, r2) that are immersed in a test fluid. The bubbling of the gas through the probes produces a differential pressure signal (ΔP) which is directly related to the surface tension of the liquid. The surface tension can be calculated by using the Young-Laplace equation in the reduced form for spherical bubble shape within the liquid.

5. RESULTS AND DISCUSSION

5.1. Polyaniline metal salt composite for H_2S gas sensing

Metal salts form complexes with polyaniline. These complexes are formed through the coordination of the metal cation to the nitrogen atoms of both benzenoid and quinoid groups.[43] The composite of copper chloride with polyaniline has been reported to be more sensitive towards H_2S gas than other PANI-metal salt composites. The sensing of H_2S gas by a composite of polyaniline and copper chloride can be explained by the formation of copper sulfide and hydrochloric acid, where the mineral acid protonates the emeraldine base PANI and leads to an increased conductivity (i.e. decrease in resistivity).[101, 102]

5.2. Development of polyaniline metal salt to an ink formulation

The commercially available powder of polyaniline emeraldine base (PANI EB) and an aqueous dispersion with 10% by weight polyaniline emeraldine salt (PANI ES) were used as starting materials. The inks were optimized for H_2S gas sensing functionality in terms of polyaniline concentration, metal salt concentration, pH and stability of the dispersion in the presence of metal salt.

PANI EB powder is insoluble in aqueous medium while it's soluble in a number of organic solvents like m-cresol, dimethyl acetamide, dimethyl formamide, dimethyl sulfoxide and n-methyl-2-pyrrolidone (NMP). Dispersions containing different concentrations of PANI EB and copper chloride (CC) in NMP were made. The sensing films were prepared by depositing a drop of 5, 10 and 20 µL of PANI EB/CC dispersions on top of inkjet-printed interdigitated silver electrodes. The sensitivity of the sensor towards H_2S was optimized in terms of PANI EB concentration and CC concentration (Paper I). After optimization the sensor showed more than three orders of magnitude change in resistance upon exposure to 10 ppm H_2S (paper I). The results obtained were comparable to the best results reported for corresponding sensors on non-absorbing substrates using special PANI particle morphologies. While special morphologies of PANI (nano-fibers) have been used as sensing films which have relatively large surface area for enhancing the H_2S gas sensitivity, we have demonstrated in paper I that by using a porous substrate like paper similar results can be achieved by conventional PANI through optimization of the PANI and metal salt concentration.

The development of the synthesis procedures enabled the production of stable aqueous dispersions of polyaniline emeraldine salt form.[103] Aqueous dispersions of PANI are more favourable compared to dispersions in organic solvents in terms of

toxicity and boiling point of the solvent. In paper II, aqueous dispersions of PANI (2.5 wt.%) with a native pH of 2.4 were optimized in terms of pH and CC content. The drop-casted films were dried in an oven at 60 °C for two hours prior to exposure to H_2S. Figure 14a shows the response of the sensors to H_2S gas. The largest responses were observed for CC concentrations in the range 0.06 to 0.12 M, and at pH values in the range 5 to 9. The resistance of these films decreased more than four orders of magnitude once exposed to H_2S. The pH and CC concentration dependency can be understood based on the known pH dependency of the PANI protonation, the influence of CC concentration on PANI dispersion stability, and the formation of $Cu(OH)_2$ at high pH. At CC concentrations exceeding 0.12 M, clear indication of phase separation was evident in turbidity measurements, to an extent which was CC concentration dependent. At lower CC concentrations no sign of phase separation was observed within 10 hours (Figure 14b). In Figure 14b, the x-axis represents the height of the glass tube. In the dispersion with 0.12 M $CuCl_2$ no instability like phase separation, sedimentation or flocculation was seen, whereas for the dispersion with 0.24 M $CuCl_2$ a clear phase separation was apparent with an increase of the transmission signal (height range 25 to 40 mm).

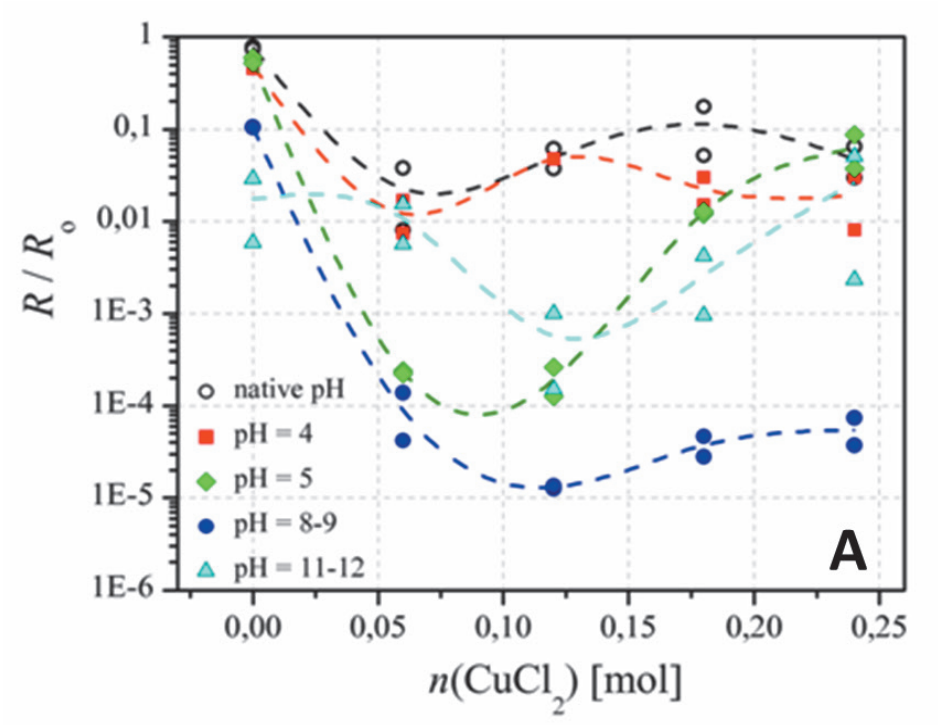

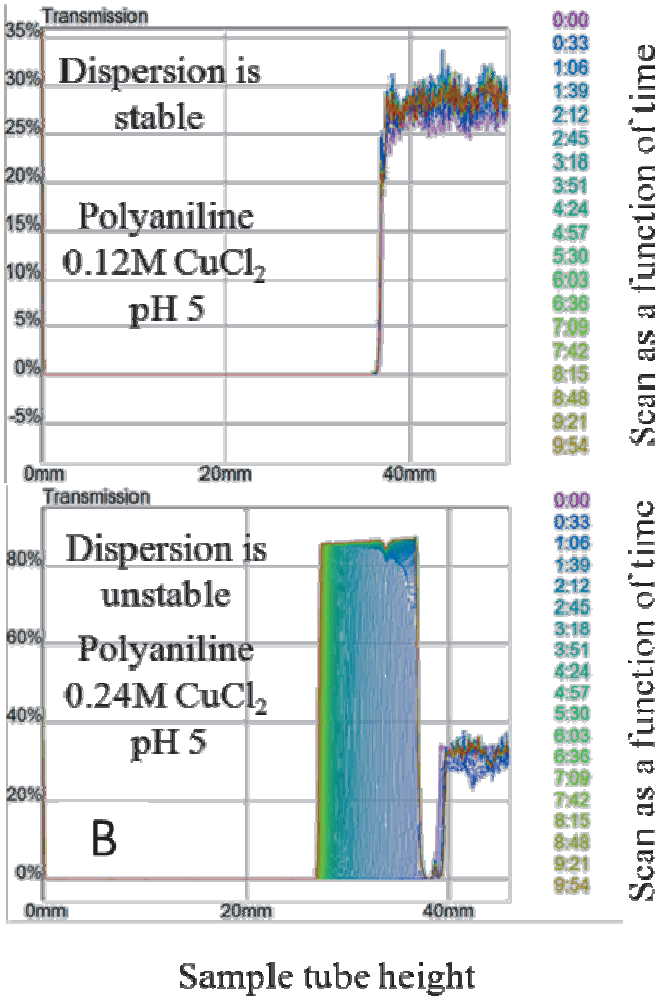

Figure 14 (a) The response of the drop-casted PANI films to H_2S exposure as a function of salt concentration and pH. The films were exposed to 15 ppm H_2S for 90 min at 40% relative humidity. (b) Dispersion stability of PANI (2.5wt.%) at pH 5 with different concentrations of $CuCl_2$.

Cu^{2+} is a Lewis acid but it is not as strong as H^+. When a copper salt is added to PANI, the nitrogen which has a free doublet may create heteropolar donor bonds. The formation of such coordination complexes requires severe distortion of PANI chains and minimizes the possibilities of conformational deformations, which will contribute to decrease the electronic conductivity in the range of pH from 2.5 to 4.[104] It is also shown in the literature that PANI loses its redox activity at pH > 4.[105] Furthermore, at pH > 4, the low concentration of H^+ limits the degree of protonic doping, and the role of Cu^{2+} as an electron acceptor may become favourable that might explain the higher conductivity observed as in the case of pH from 5 to 9.[104] At pH > 8 the sensing response was poor because of the possible precipitation of

$Cu(OH)_2$ in combination with partial protonation of the sensing films upon exposure to H_2S.

In the absence of CC there was almost no response of PANI towards H_2S at pH < 5, while a small response of around one order of magnitude was observed above pH 5. This behaviour may be attributed to the partial protonation of deprotonated PANI by H_2S. The exposure of pure CC films to H_2S did not lead to any changes in film resistance and thus the decrease in resistance can be positively related to the indirect protonation of PANI by H_2S through the formation of copper sulfide.

It was shown in paper II that a PANI/CC composite deposited on paper exhibited a more than four orders of magnitude change of resistance upon exposure to 15 ppm H_2S. However, the aqueous PANI/CC dispersion was unstable at neutral pH and the optimum pH range was between 5 and 8. It has been reported in the literature that copper forms stable complexes with organic acids like citric acid (CA) and the strength of a copper-CA complex is dependent on pH.[106, 107, 108] The stability and H_2S gas sensitivity of a copper-CA complex at different pH with or without PANI was studied in paper III. Cu^{2+} ions form strong complexes with organic acids.[109] CA is a fairly strong, multifunctional carboxylic acid which forms water-soluble complexes with many multivalent metal ions.[110, 111] The stability of the copper complex with CA depends upon many parameters like copper salt concentration, CA concentration, copper salt to CA ratio, pH etc. In paper III the mixtures containing 1M CC and 1M CA with a volume ratio of 1:1 were used. The stability of these mixtures was studied at native pH 0.5 and pH 6. The viscosity of the mixture was tuned to be in the optimum range for inkjet-printing by using a mixture of water (W) and ethylene glycol (EG) with a volume ratio of 7:3 to yield a viscosity of 1.9 mPa s at 25 °C. The pH of the mixture was adjusted by using NaOH solution. The stability of the CC/CA mixture in W/EG at native pH 0.5 and pH 6 was determined with Formulaction Turbiscan MA2000. The concentration of copper chloride and citric acid was 0.5M in the mixture. The mixtures were stable over a time scale of twenty hours as no precipitation or phase separation was observed.

In paper III, respectively, the stability of the PANI dispersion in the presence of CC and CC/CA mixture as a function of pH was studied. A clear phase separation can be seen in the PANI dispersion with CC at pH 6 with a composition of the mixture being 7.5 mL of 10%wt PANI + 2.5 mL of 1M CC as shown in Figure 15c. The instability appears as an increase in transmission (already after 1.5 hours) in the Turbiscan spectra. Furthermore, a clear phase separation can be seen in the inset picture in Figure 15c. Figure 15d shows a schematic illustration of the unstable dispersion (phase separation) in the Turbiscan measurement tube. The light colour shows the clear supernatant while the dark colour refers to the flocculated dispersion. This instability of the dispersion limits the possibility of roll-to-roll printing. However, by using a CC/CA mixture instead of CC in the PANI dispersion the stability of the mixture was improved significantly. The PANI dispersions with

CC/CA with a composition of the mixture being 5 mL 10%wt PANI + 5 mL mixture of CC (1M) CA (1M) at pH 6 and pH 8 were stable for more than 20 hours. The Turbiscan spectra measured at pH 6 are shown in Figure 15a. No phase separation was observed as shown in the inset picture in Figure 15a. Figure 15b shows the schematic illustration of the stable dispersion (no colour change in this case) in the Turbiscan measurement tube. It is worth mentioning here that the mixture containing PANI/CC-CA at pH 6 was stable even with more CC per amount of PANI in the mixture compared to the PANI/CC mixture at pH 6.

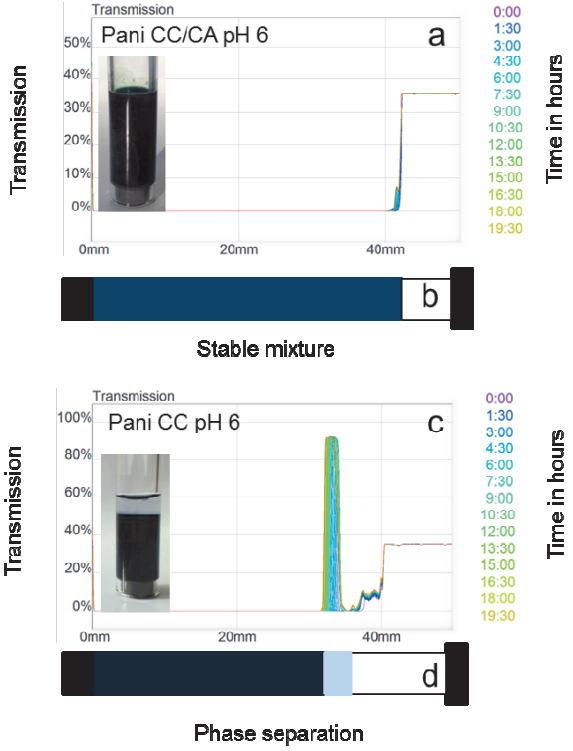

Figure 15 Turbiscan spectra of (a) a PANI-CC-CA mixture at pH 6 and (b) a schematic illustration of the stable dispersion in the Turbiscan measurement tube. (c) Turbiscan spectra of a PANI-CC mixture at pH 6 and (d) a schematic illustration of the unstable dispersion in the Turbiscan measurement tube. The light colour shows the clear supernatant while the dark colour indicates the flocculated dispersion.

5.3. Electrical response of the polyaniline composite based H_2S gas sensors

Sensors can be manufactured using different coating and printing methods such as drop-casting, screen printing, spray coating, inkjet printing etc. The sensors in paper I were made by drop-casting the optimized PANI EB/CC dispersion in NMP on inkjet-printed silver electrodes (the distance between the fingers of the interdigitated

electrodes was 100 µm). In paper II the sensors were made by drop-casting, screen printing and spray coating the optimized PANI ES/CC dispersion on inkjet-printed silver electrodes (the channel width in the interdigitated structure was 100 µm). In paper III roll-to-roll printed sensors were made by flexographically printing the optimized PANI ES/CC-CA dispersion on top of flexographically printed interdigitated silver electrodes (with line gap of 500 µm between the interdigitated electrodes). The electrical response of these differently manufactured sensors towards 10 - 15 ppm H_2S is compared in Figure 16.

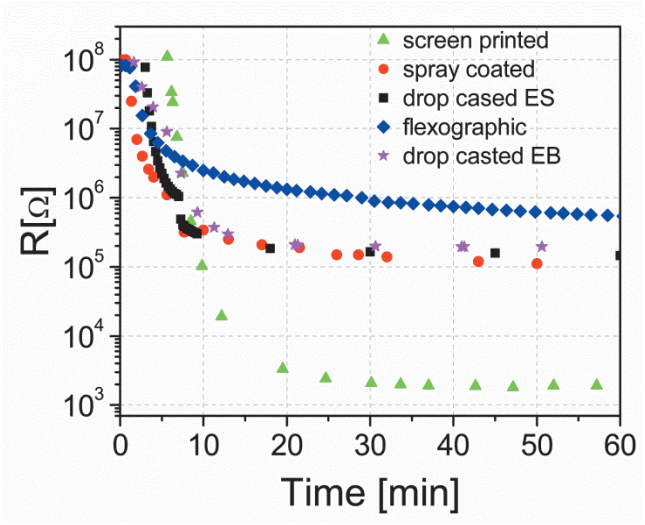

Figure 16.The electrical response of the drop casted, screen printed, spray coated and flexographically printed sensors towards H_2S exposure.

The resistance of the sensor dropped after the exposure to H_2S, as a result of the conversion of PANI from a nonconducting state to a conducting emeraldine salt form, accompanied by the formation and growth of CuS particles (to be discussed in detail in the characterization section). The sensing response obtained for the drop-casted and spray-coated sensors is quite similar. The differences in the sensing response between the screen-printed and spray-coated sensors can be explained in terms of film thickness (section AFM characterization). Thin films were better in sensing the H_2S gas, which can be explained by the easier diffusion of the analyte molecules from the surface to the bulk.[112] The differences in the sensing response of the flexographically printed sensors and screen-printed sensors may be speculated to be due to the difference in the geometry and gap between the fingers of the interdigitated silver electrodes. The gap between the fingers of the flexographically printed interdigitated silver electrodes was five times larger than that of the inkjet-printed electrodes which might explain the relatively poor response of the flexographically printed sensor.

5.4. Characterization

5.4.1. Analysis of the structure of the sensor surfaces with TEM

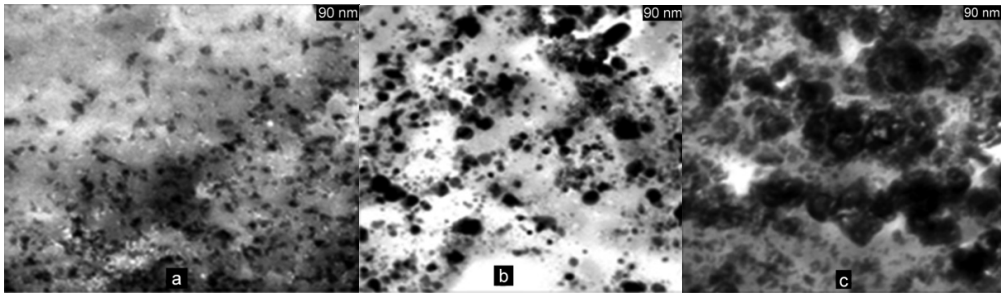

Figure 17. Drop casted PANI-$CuCl_2$ films: (a) unexposed reference, (b) H_2S-exposed at 20 ppm for 2 hours, and (c) H_2S-exposed at 60 ppm for 30 hours at RH 45%. The length bar is 90 nm.

TEM investigations were performed on drop-casted PANI ES/CC composite films as a function of H_2S concentration and exposure time. In order to be able to have a better resolution for the Cu-species, we used polyethylene terephthalate (PET) as the substrate, and also employed higher H_2S concentrations. The TEM images are shown in Figure 17. Before exposure to H_2S, the CC particles were well dispersed with a particle size of 10 to 20 nm and evidently poorly connected to each other in the PANI film. These particles grew and aggregated with time and increasing H_2S concentration to end up in aggregates of about 100 nm in size upon formation of CuS. The aggregates became interlinked and formed continuous CuS networks in the film. The increased conductivity of the film can be explained by the percolation[113] in the continuous conducting networks[114] between the isolated conducting particles which can be seen in Figure 17. However, the paper substrates were more porous than the PET films used in the TEM investigations, which may lead to less pronounced particle growth and differences in the extent of percolation. However, on a descriptive level we conclude that the behaviour is similar in both cases.

5.4.2. AFM characterization

In order to have better understanding of the observed sensor responses (Figure 16), we performed structural characterization on the spray-coated and screen-printed sensors. AFM images of the used substrate and the sensor structures are shown in Figure 18.

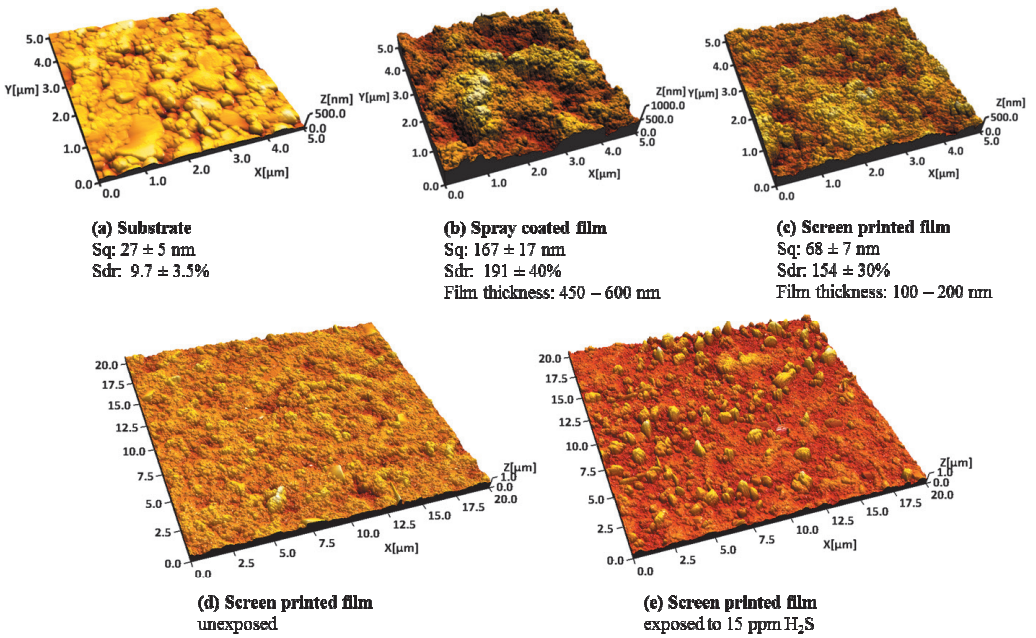

Figure 18. AFM images (5µm x 5µm) of (a) a paper substrate (b) a spray-coated film and (c) a screen-printed film. (d) Larger scale (20µm x 20µm) AFM images of the screen printed film before and (e) after H_2S exposure.

The AFM topographs show that both the spray coated and screen printed films had fully covered the surface of the paper substrate since the characteristic structure of the pigment coating is no more visible. The polymer films were rougher and had larger surface area compared to the paper substrate as indicated by the S_q and S_{dr} values given below the corresponding topographs. The deposition method had an effect on the thickness and roughness of the film. Spray-coating resulted in a considerably thicker and rougher surface compared to the screen-printed film. This may be partly due to the differences in the deposition amounts. The effective thickness of the PANI layer was determined from an AFM line profile obtained over the print-substrate border area by calculating the difference between the mean plane value of the substrate and the average height value of the PANI layer. Local variations in the PANI layers were observed to a varying degree in each sample. However, no significant coffee-ring (when a drop evaporates, fluid flows outwards carrying particles from the middle of the droplet to its edges and leaves behind a ring like stain called coffee-ring) formation was observed with any of the samples.

Figure 18 (d) and (e) illustrate the surface structure of the screen printed PANI/CC films. In accordance with the TEM images (Figure 17) similar type of particle (CuS) growth can be seen after exposure to H_2S.

5.4.3. XPS Characterization

The survey spectra measured for the H_2S-exposed and unexposed PANI ES/CC composite based sensors differed clearly regarding the copper and the sulphur peaks. The new peaks that emerged after exposure to H_2S were identified as S2p and S2s, where the sulphur was most probably bound to Cu in the form of Cu_2S.

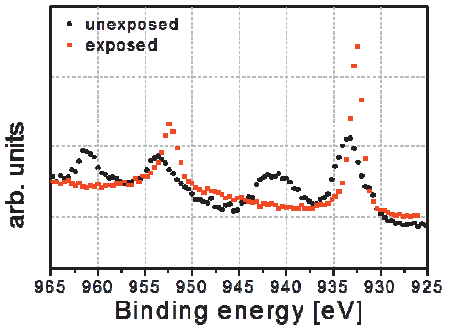

Figure 19. XPS high resolution spectra of Cu for the unexposed and H_2S-exposed (15 ppm, 2 hours) films.

Figure 19 shows the high resolution spectra of Cu before and after exposure to H_2S. After exposure, copper had been reduced from Cu (II) to Cu (I) as the "shake up" satellite was not visible anymore.[115] Cu "shake up" satellite peaks were visible in the spectra of the unexposed sample with the binding energy between 937 eV to 945 eV. The copper 2p peaks for the exposed sample were located at 932.5 eV and 952.4 eV which corresponds well to copper sulphide (Cu_2S). The peaks also have a doublet separation of 19.9 eV, as previously reported in the literature. [116]

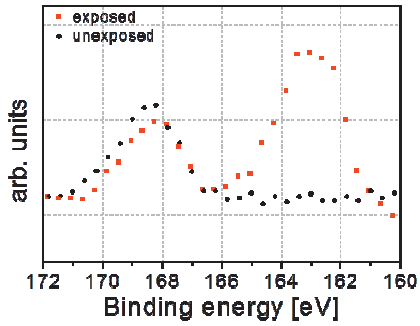

Figure 20. High resolution XPS spectra of sulfur for the unexposed and H_2S-exposed (15 ppm, 2 hours) sensor films.

Figure 20 shows the high resolution peaks of sulfur for the H_2S-exposed and unexposed films. A clear sulfur peak was present even before exposure to H_2S at a binding energy of 168.3 eV. The source of the sulfur peak was most probably the dodecylbenzenesulfonic acid which is a common dopant used during the synthesis of

PANI ES.[117] After exposure the formation of a new peak around 163 eV indicates that sulfur was most probably bound to copper in the form of Cu_2S.[118] The peak at 168.3 eV appears with almost the same intensity as before exposure. Besides originating from the dopant, the peak may also be attributed to a surface layer of sulphate formed as a result of exposure to H_2S.[119]

5.4.4. Sensor characteristics

The characteristics of the produced sensors like stability, cross sensitivity, reversibility, repeatability, reaction kinetics and onset time of detection were studied and discussed in detail in papers II and III. Briefly, all the sensors behaved irreversibly probably because of the formation of Cu_2S which is fairly stable at room temperature. Both the reaction kinetics and onset time of detection of the sensor depend on the film thickness and the geometry of the interdigitated electrode structure. The PANI/CC composite sensor exhibited good repeatability with a coefficient of variation of 3 % at a saturation level (with S = 56 and $\bar{x}$ = 1840) under room temperature at 45 % relative humidity conditions as shown in paper II.

The cross sensitivity of the PANI/CC based sensor was also studied in paper II. The H_2S gas sensor is often sensitive to other sulfur-containing compounds.[120] Considering sensor applications in food quality and safety the most common interfering gases to be considered are CO_2, humidity, NH_3 and sulfur-containing compounds. The cross sensitivity of the spray-coated CC-modified PANI sensor was tested towards SO_2, CO_2 and high RH (60%) (Figure 21). The sensors exhibited no response towards CO_2 but they showed slight sensitivity towards SO_2 and higher humidity. Figure 21 shows that the change in resistance of the sensor towards H_2S was at least two orders of magnitude more than the tested interfering gases. In addition, the sensor showed much faster response (short onset time) towards H_2S compared with the other tested gases.

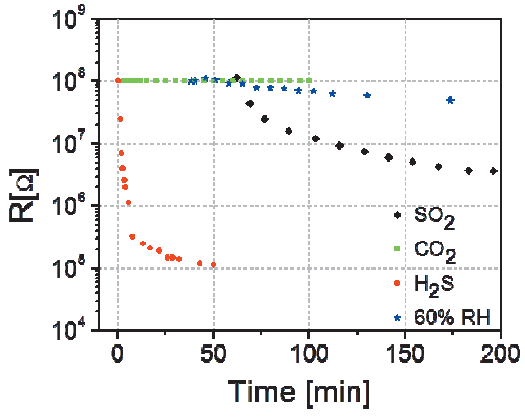

Figure 21. The response of the spray-coated copper chloride modified PANI sensor towards SO_2, CO_2, H_2S and high relative humidity.

5.5. H_2S sensor based on copper acetate

Different sensors, including those based on pure and doped metal oxides, optical sensors and electrochemical sensors have been reported in the literature in order to sense H_2S.[121, 122] The main disadvantage with these materials is their high required operating temperature. Composites of conducting polymers with metal salts have also been shown to be potential H_2S gas sensing materials. These composite materials show large changes of conductivity when exposed to H_2S at room temperature. The humidity background and long-term stability of these devices are still a question mark.[43] In recent years metal salts of organic acids have been studied for sensing H_2S gas. Among them, CuAc has shown promising results.[123] CuAc films show large changes in the conductivity upon H_2S gas exposure, which can be related to the difference in the conductivity of the metal salt and the resulting metal sulfide. CuAc reacts with H_2S both in solution and in solid state.[123] It reacts with H_2S in water to produce a black precipitate of copper sulfide,[124] while in organic solutions it produces organosols.[125] CuAc films have also been reported to react directly with H_2S to form copper sulfide.[126] The electrical response of CuAc films towards H_2S has been reported earlier by Virji et.al.[123]

5.6. Development of a copper acetate based ink for inkjet-printing

In paper IV CuAc solutions were made with equal concentration of CuAc in pure and mixed solvents using water, iso-propanol (IPA) and ethylene glycol (EG). To study the effect of solvents on H_2S sensing properties, drop-casted films were prepared on inkjet-printed interdigitated silver electrodes (the channel width in the interdigitated structure was 40 μm) and were exposed to 10 ppm H_2S. The electrical response of the films is shown in Figure 22. A film casted from a CuAc solution in water/EG/IPA clearly showed the fastest response against H_2S. The resistance of the film dropped more than seven orders of magnitude in less than 30 minutes, whereas the CuAc film prepared using IPA as the solvent gave a measurable response only after about 30 minutes of exposure to H_2S and the resistance decreased only about four orders of magnitude. This less pronounced response could be because of the poor solubility of CuAc in IPA. The optimum conductivity response was obtained for the film made from a 0.1 M CuAc solution with mixed solvents (water, ethylene glycol, iso-propanol). In addition, the optimized ink had the best printability in terms of surface tension and viscosity. This optimized ink was later used for inkjet printing of the sensing device. The ink properties of the studied inks are collected in Table 3.

Table 3. Ink properties of the studied copper acetate solutions.

0.1M CuAc solution in	Surface Tension [mN/m]	Particle size [nm]	Dynamic viscosity [centipoise] at 25ºC
Water	72	< 200nm*	0.87
water/EG	63	< 200nm*	1.9
water/IPA	32	< 200nm*	1.7
water/EG/IPA	40	< 200nm*	1.92

* Ink filtered with a 200 nm filter before printing.

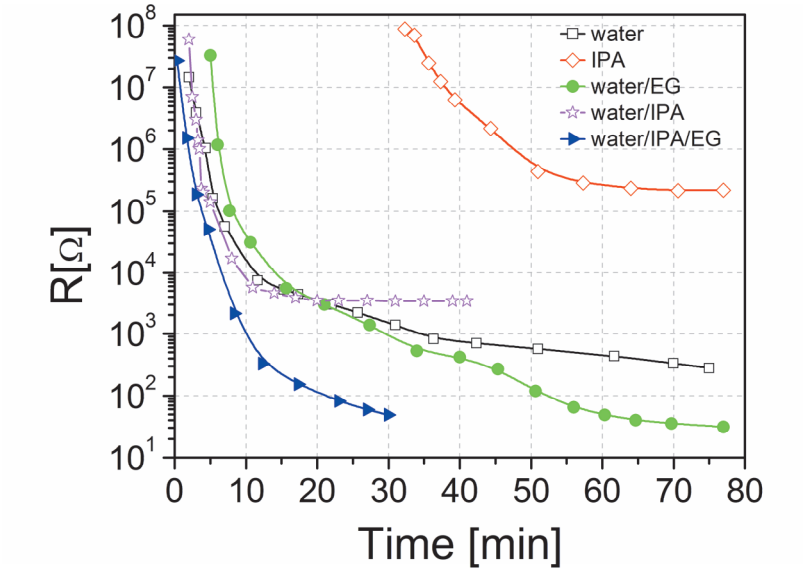

Figure 22. The change in resistance of films of copper acetate drop-casted on a paper substrate from solutions with different solvents, when exposed to 10 ppm H_2S at a relative humidity of 40%.

5.6.1. TEM characterization

Figure 23 shows the TEM images of unexposed and exposed CuAc films on PET, the films were made from a 0.1 M solution of CuAc in water. The size of the particles is directly comparable since the image size is the same. Upon exposure to H_2S the size of the particles started to grow as a result of the formation of Cu_2S. With growth of the particles they formed a conductive path which resulted in a decrease of resistance of these sensors. The increase in size of the particles was dependent on the exposure time and the concentration of H_2S. The increase in conductivity of the film (Figure 22) can be explained by the percolation[127] in the continuous conducting networks[114] between the isolated conducting particles. Cu_2S crystals started to form (Figure 23) after exposure of these films to H_2S. The paper substrates are more porous than the PET films used in the TEM investigations, which may lead to less pronounced particle growth and differences in the extent of percolation.

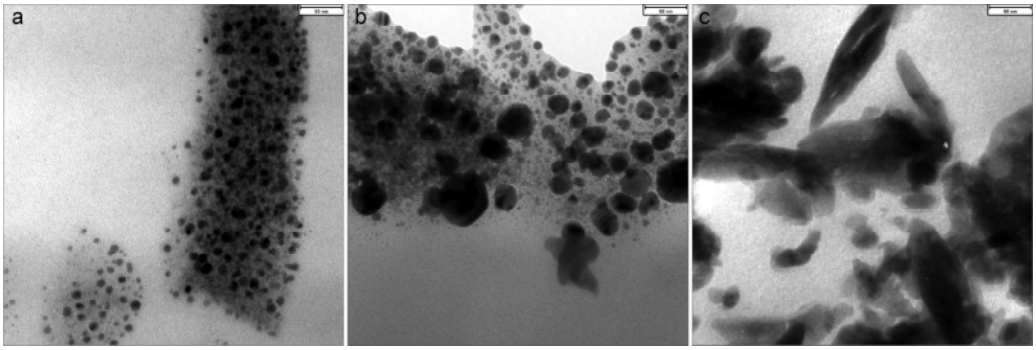

Figure 23. A drop casted copper acetate film made from 0.1 M copper acetate solution in water on a PET substrate; (a) The unexposed reference, (b) the film exposed to 20 ppm H_2S for 2 hours, and (c) the film exposed to 60 ppm H_2S for 30 hours. The length bar is 60 nm in each image.

5.6.2. XRD characterization

To study the formation and growth of copper sulfide crystals during the reaction of CuAc with H_2S, drop-casted films of CuAc on a glass substrate were exposed to different concentrations of H_2S for one hour at 40 % relative humidity. All the films were prepared by drying a drop of CuAc solution on a glass slide at 60 °C for two hours. The XRD spectra are collected using Grazing-incidence diffraction and are shown in Figure 24.

The obtained XRD pattern matches the reference file for copper sulfide (CuS) covellite phase with peaks at 27.2°, 29.3°, 31.9°, 32.7° and 48°.[128] Covellite CuS belongs to the group of binary copper sulfides, which have the formula Cu_xS_y and can have a wide-ranging copper/sulfur ratio from 1:2 to 2:1 (Cu/S).[129]

The XRD data confirms the formation of CuS crystals. It can be seen from Table 4 that the particle growth increases with increasing concentration of H_2S. The crystal size and the crystallinity of the films are also included in Table 4. The grain size in the copper sulphide thin films is calculated by using the Scherer's relation: $D = 0.9\lambda / \beta \cos \theta$, where D is the crystallite size, λ is the wave length of the x-rays, θ is the Bragg angle and β is the peak width at half of the maximum intensity (FWHM). The table shows that upon exposure to 20 ppm H_2S for one hour almost 60 % of the amorphous phase had been converted to crystallites. On the other hand, only 15 % of the crystallites were formed when the similar film was exposed to 5 ppm H_2S for one hour. Similarly, the crystal size for the unexposed reference sample was 1 ± 0.3 nm (calculated by AFM) which increased to 20.4 nm after exposure to 20 ppm H_2S for one hour.

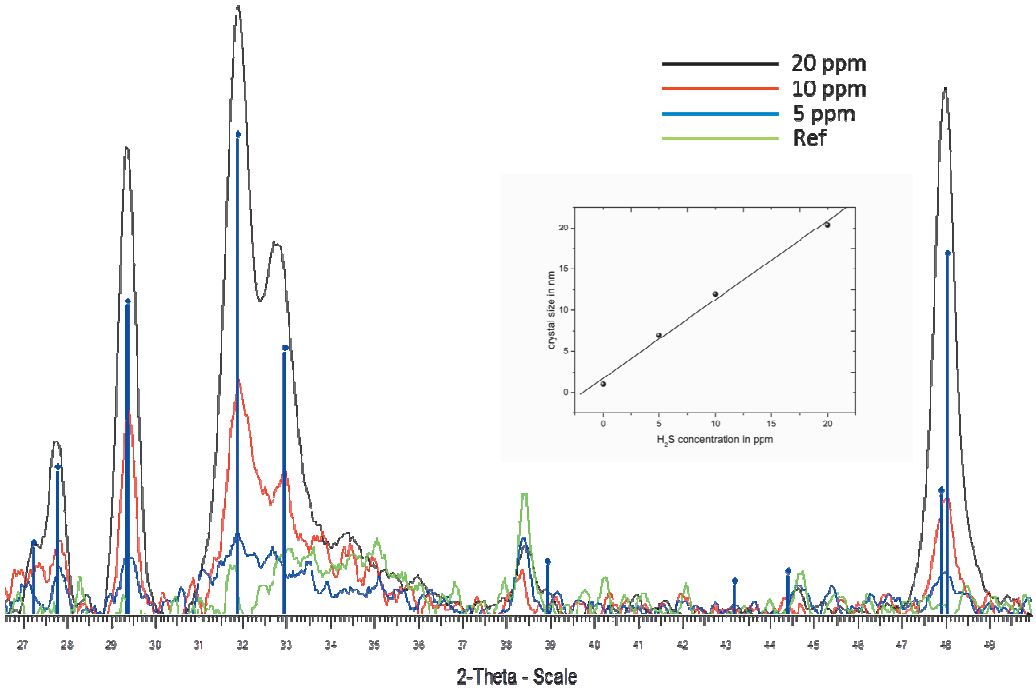

Figure 24. GID spectra of the drop-casted copper acetate film on a glass substrate exposed to different concentrations of H_2S for one hour at 45 % relative humidity. The obtained GID spectra match with the copper sulfide (CuS) covellite phase pattern. The inset shows the increase in the crystal size as a function H_2S concentration.

Table 4. The crystal size and crystallinity of the drop-casted films on a glass substrate.

2θ	H_2S concentration (ppm)	Crystal size (nm)	Crystallinity (%)
28.76 – 29.86	20	20.4	58
28.97 -29.408	10	12	26
29.15 – 29.59	5	7	15
REF mica	0	1±0.3	

5.6.3. XPS characterization

Figure 25 shows the XPS spectra of inkjet-printed CuAc films on a paper substrate before and after exposure to H_2S. Similar to the PANI-based sensors, new peaks at 932.5 eV and 952.4 eV emerged after exposure to H_2S, corresponding to the S2p doublet peak, where the sulphur is most probably bound to Cu in form of Cu_2S. Figure 25b shows that the exposure caused the reduction of copper from Cu(II) to Cu(I).[115] Cu $2p^{3/2}$ and Cu$2p^{1/2}$ peaks were visible in the spectra for the unexposed sample. In the unexposed sample the peak position 933.5 eV indicated that copper was most probably in the form of CuO at the surface of the printed sensor.[130] The shift of the peak of

copper from 933.5 eV to 932.5 eV in Figure 25b indicates the conversion of CuO to Cu_2S. Figure 25a shows the high resolution spectra of sulfur, which bound to copper in the form Cu_2S.[118] The formation of a sulphate layer[131] (peak position at 168 eV) due to oxidation of the surface layer was also evident. As a difference to the PANI-based sensor, no background peak for sulfur was observed for the unexposed film.

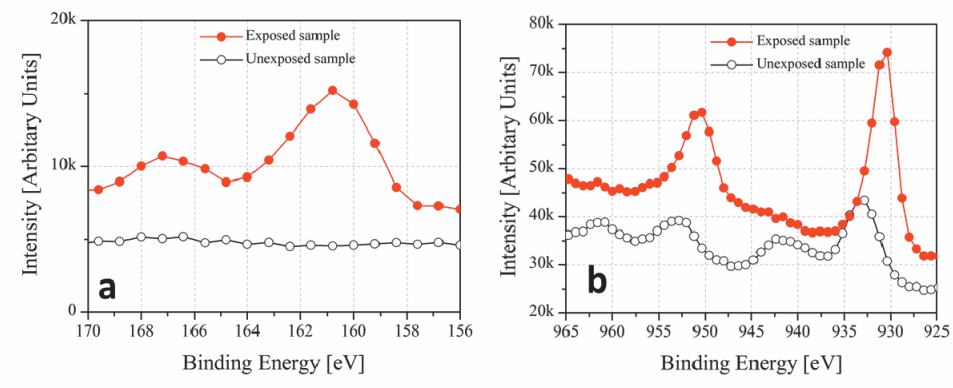

Figure 25. XPS spectra of the sensors unexposed and exposed to H_2S showing (a) sulfur peaks and (b) copper peaks.

5.6.4. Sensor characteristics

In paper V the performance of the gas sensor was verified by studying the parameters like sensing kinetics, onset time of detection, long term stability, selectivity, cross sensitivity, humidity effects and repeatability. The sensors were prepared by inkjet-printing of the optimized CuAc-based ink on paper substrates with inkjet-printed interdigitated silver electrodes (with channel width between the fingers being 100 µm). The CuAc solution was made by dissolving the salt in mixed solvents for a final concentration of 0.1 M. Water, ethylene glycol (EG) and iso-propanol (IPA) were used as solvents. A volume ratio of 8:1:1 was used for water/EG/IPA. The ink was filtered using a 200 nm polypropylene filter before printing.

5.6.5. Sensing kinetics

The sensitivity of a sensor is the ability to detect small concentrations of analyte, that is how much the sensor output (resistance in our case) changes when the measured quantity (analyte concentration) changes. In this study, since the changes in resistance of the sensor are more than eight orders of magnitude and the final resistance values are so small compared to the initial values, the sensitivity in terms of normalized ratio ($\Delta R/R_O$) is almost equal to one in all cases. In this case it is more relevant to discuss the sensing kinetics of the sensor rather than the sensitivity in absolute terms.

A set of H_2S concentrations ranging from 1 ppm to 20 ppm were selected to study the response of the sensor. A 45 % relative humidity was recorded during the

measurements. The low concentration range (1 - 20 ppm) of H_2S was selected bearing in mind the practical applications of these sensors in for example food packaging and environmental monitoring. Two types of sensors, sensor A (three printed layers of the sensing material) and sensor B (two printed layers) were studied. Figure 26a shows the sensing response of inkjet-printed sensors A as a function of time for different H_2S concentrations.

Figure 26b yields the detection rate (slope = $\Delta R/\Delta t$) of A-type and B-type sensors as a function of H_2S concentration. Figure 26b shows that at higher concentration, 20 ppm, both sensors have a higher detection rate towards H_2S (steeper slope), i.e. they show fast kinetics compared to low concentration, 1 ppm. The detection rate decreases linearly with the decrease in the concentration of H_2S for both sensor types. Figure 26b also shows that sensor A has in average 20 times faster a detection rate than sensor B.

5.6.6. Onset time of detection

Figure 26a also shows that the onset time of detection for sensor A increases from 3 min to 45 min with decrease in the H_2S concentration from 20 ppm to 1 ppm. Figure 26a further show that the saturation level achieved after being exposed to different concentrations of H_2S was not constant. These differences in the saturation level might be explained by the heterogeneous substrate, printing variations, and the differences between the formation and connectivity of the copper sulfide particles upon reaction of CuAc with H_2S.

The sensing response of the inkjet-printed sensor B towards different concentrations of H_2S was also studied (data not shown). Sensor B showed a similar trend as sensor A in terms of onset time of detection, response time and kinetics. However, the onset time was almost doubled as compared with sensor A.

The substrate roughness is presumed to explain the differences between the responses of the two sensor types. The two printed CuAc layers in sensor B may not be enough to form a continuous film because of incomplete filling of the pores of the substrate. The enhanced performance observed for the three printed layers can be explained by the better coverage of the electrodes and by the formation of a continuous sensing film.[132]

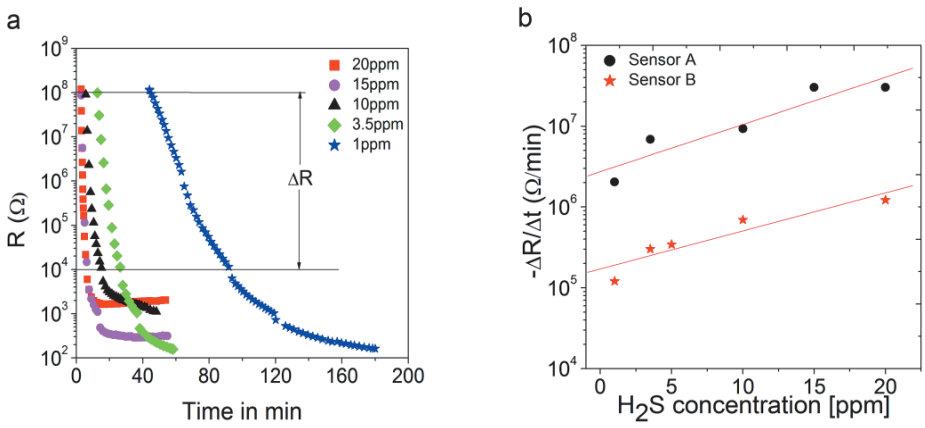

Figure 26(a)The response kinetics of inkjet-printed A-type sensors towards different H_2S concentrations, and (b) the detection rate of Sensor A and B as a function of H_2S concentration.

5.6.7. Long term stability of the sensors

The change in resistance of the unexposed sensor A and B was followed over a course of 57 days storage at ambient conditions (with RH varying within 40 % ± 10 %). During the storage, the resistance of the unexposed sensors increased from their initial value 1 GΩ (measured on the day of printing) to around 100 GΩ. This effect is explained by the drying of the sensing films over time.

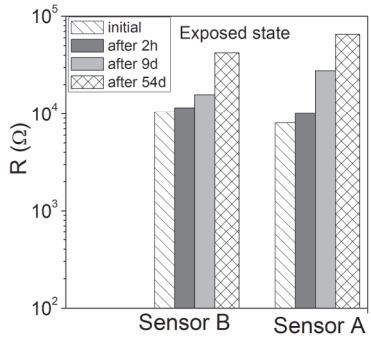

Figure 27. The change in resistance of the H_2S-exposed sensor A and B during 54 days storage in ambient air.

The stability of the H_2S-exposed sensors in terms of change in resistance was also studied over a course of 54 days storage in ambient air. It can be seen in Figure 27 that the resistance of the sensors has increased less than an order of magnitude during 54 days which might be because of the surface oxidation of copper sulfide. In any case, the instability can be regarded rather small compared with the nine orders of magnitude change in resistance of these sensors upon exposure to H_2S. Figure 27 show that the sensor behaves as an irreversible (memory-type) chemiresistor, i.e. the resistance does not recover towards the initial value.

5.6.8. Selectivity and cross sensitivity

The cross sensitivity of sensor A was tested towards SO_2, CO_2, and CH_3NH_2 (methyl amine). The sensor exhibited no electrical or optical response towards either CO_2 or SO_2 during two hours of exposure (data not shown).

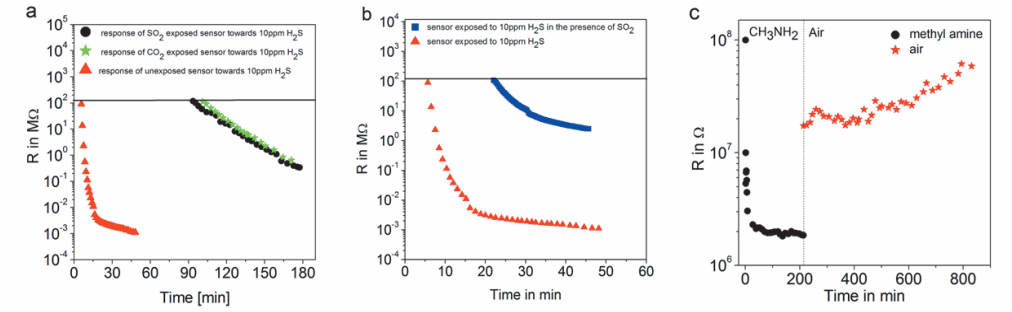

Figure 28. (a) The electrical response of unexposed and SO_2, CO_2 exposed sensors A towards 10 ppm H_2S. (b) The response of sensor A exposed to H_2S (10 ppm) in the presence and absence of SO_2. (c) The response of sensor A towards methyl amine.

Figure 28a shows that the sensor is still sensitive towards H_2S even after having been earlier exposed to SO_2 and CO_2 for two hours. However, the increase in the onset time of detection for H_2S (from 5 min to 94 min) and the decrease in detection rate towards H_2S (from -9.3×10^6 to -1.6×10^6 Ω/min) were quite obvious.

The response of the sensor towards H_2S (10 ppm) in the presence of SO_2 showed a longer onset time of detection and slower response compared to the response in the absence of SO_2 (Figure 28b). The relatively slow response exhibited by the sensor could be because of competing adsorption between H_2S and SO_2 and might arise from the formation of an adsorbed layer on the sensor surface by the interfering gas.

Figure 28c shows the response of sensor A to methyl amine. The resistance of the sensor decreased almost two orders of magnitude upon exposure to methylamine. However, the observed change in resistance is still relatively small compared with the response to H_2S gas (more than eight orders of magnitude). In addition, the sensing response is different from that of H_2S. The sensor behaves reversibly towards methyl amine; once the gas flow was ceased the resistance of the sensor immediately recovered to a higher resistance level and then slowly approached towards its initial level.

The decrease in the resistance of the sensor upon exposure to methyl amine may be explained by the complex formation of CuAc with methyl amine and possible reduction of copper. A large number of adducts of copper (II) carboxylates exist with stoichiometry $Cu(RCO_2)_2$ - L, where L is a donor molecule such as water or amine. Many of these compounds are better formulated as $Cu_2(RCO_2)_4$ - L_2 with the copper atoms held together by bridging carboxylate groups.[133 – 136] The sensors being exposed to methyl amine were later exposed to H_2S for two hours. No electrical response was

obtained from the sensor possibly because of the complex formation of CuAc with methyl amine which indicates that amine-based compounds have an electrically passivating effect on the CuAc layer.

5.6.9. Humidity

The influence of humidity on the performance of the sensor is very important since the sensor is manufactured on a paper substrate, and at high humidity (>80 %) the electrical conductivity of a paper substrate increases due to the mobility of ions. The sensor was exposed to different humidity atmospheres ranging from 14 % RH to 80 % RH. No humidity-induced background conductivity was obtained when the sensor was exposed up to 60 % RH for four hours. At 80 % RH the sensor showed a drop in resistance and stabilized at a level around one mega ohms as shown in Figure 29a.

It can be seen from Figure 29a that at 80 % RH the initial fast drop of resistance of the sensor when exposed to H_2S is a combined effect of humidity and H_2S. Furthermore by decreasing the relative humidity from 80 % to 42 % and 22 % the onset time of detection increased from 0.7 min to 3 min and 35 min, respectively. However, the reaction kinetics of the sensors at different humidity conditions was almost identical, except at 14 % RH.

At high RH, an adsorbed H_2O layer up to a few monolayers thick is present on the surface.[137] H_2S may dissolve in this adsorbed H_2O layer and dissociate into a number of possible ionic species, e.g. HS^- (aq), S_2^- (aq), H^+ (aq) etc.[137] The different ionic species appearing at different RH values most probably explain the differences in reaction kinetics and onset time of the sensor at different humidity conditions.

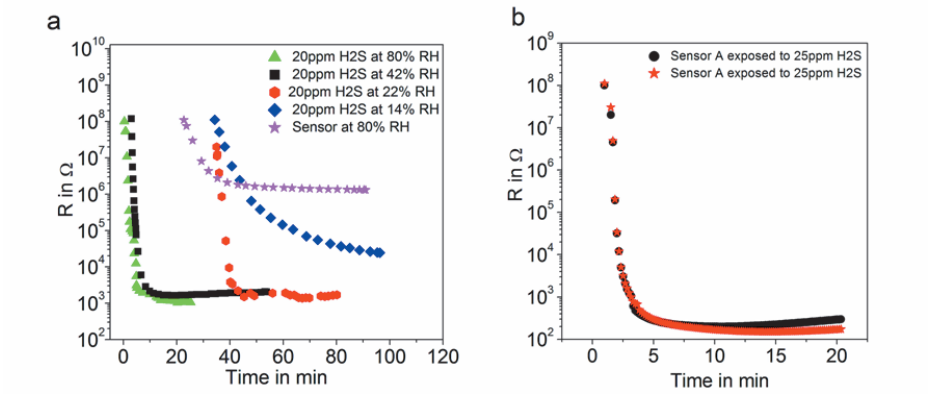

Figure 29. (a) The effect of humidity on the sensor performance, and (b) the repeatability of the inkjet-printed sensors.

5.6.10. Repeatability

Figure 29b shows the accuracy and repeatability for two separate inkjet-printed sensors (sensor A) which were exposed to 25 ppm H_2S at 45 % RH. Clearly the response in terms of reaction kinetics (the slope of the response curves) of the two sensors is nearly identical. However, the sensors saturated at slightly different levels which may arise from the heterogeneous surface and variations in print quality of the CuAc layers.

5.6.11. Incorporation of gold nanoparticles into the copper acetate films for sub-ppm detection of H_2S

In paper VI significant improvements on the onset time of detection and reaction kinetics were reported for the developed H_2S sensors through plasma treatment of printed CuAc thin films. Further improvements were gained by incorporating catalytic AuNPs into the sensing layer. The combination of plasma treatment and AuNPs enabled the sub-ppm detection of H_2S and regeneration of the sensor by subsequent plasma treatment (paper VI).

The effect of plasma treatment on the electrical response (change in resistance, R) of printed CuAc-based sensors was first tested without incorporation of AuNP in the sensing film. Figure 30A shows typical electric responses of the sensors (with inkjet-printed silver interdigitated electrode structure) exposed to 1 ppm H_2S gas concentration at room temperature with and without plasma treated CuAc film. The onset time of detection (t_{on}) and the response time to 90% of full scale (full scale from 100 MΩ to saturation level excluding onset time of detection) (t_{90}) were determined from the response curves. Plasma treatment of the CuAc film prior to exposure to H_2S gas resulted in considerable improvements of both the t_{on} and the t_{90} values compared to the untreated CuAc films. The t_{on} value decreased from 105 min to 3 min and t_{90} from 65 min to 10 min (Figure 30A). A rather slow response with a high t_{on} value of the untreated sensor could be related to the time needed for the formation of sufficient CuS particle-particle contacts. Figure 30B shows typical responses of the CuAc-based sensors fabricated using inkjet-printed gold electrodes with non-conductive layers of AuNP between the conductive interdigitated electrodes. The sensor responses with and without plasma-treated CuAc film is shown for 1 ppm H_2S exposure at room temperature (Figure 30B). The sensor without plasma treatment showed the t_{on} value of 35 min and the t_{90} value of 29 min. The plasma treatment improved the response, the t_{on} value being only 1.4 min and t_{90} around 4 min. Compared to the results obtained for sensors fabricated on bare silver (Figure 30A), significant improvements were gained by using the gold/AuNP electrodes. Although the direct comparison between the two sensors is not possible due to the differences in the geometry of the electrodes especially in the gap width (400 µm for the gold/AuNP electrodes, 100 µm for the silver electrodes), the improvements in the sensor response with the inclusion of AuNP demonstrate qualitatively the metal catalyst-enhanced effect.

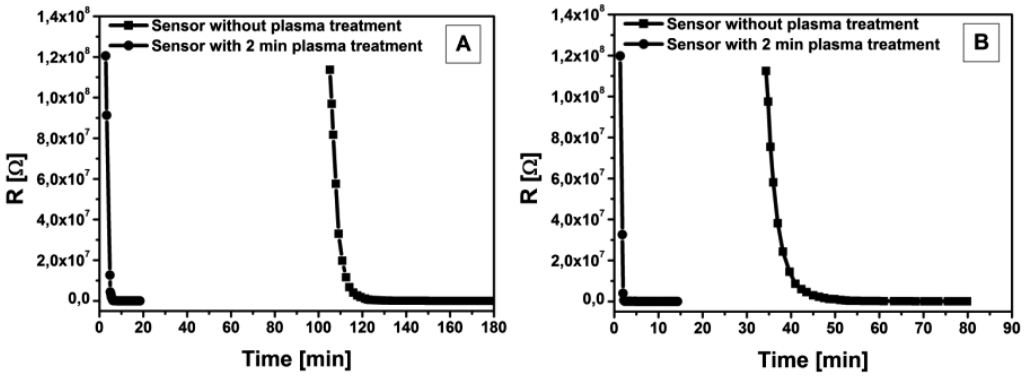

Figure 30. The electrical response (change in resistance, R) of printed CuAc-based H_2S sensors with and without plasma treatment using either (A) silver or (B) gold/AuNP electrodes when the sensor was exposed towards 1 ppm H_2S gas at room temperature with 45% relative humidity.

In addition to having the fastest response, the sensor with plasma treated CuAc film on gold/AuNP electrodes had the capability to detect sub-ppm concentrations of H_2S gas at room temperature (Figure 31A). Around four orders of magnitude change in resistance was detected at a concentration as low as 300 ppb of H_2S with t_{on} < 60 min. For comparison, no measurable electrical response was obtained from either untreated CuAc film printed on gold/AuNP electrodes or plasma-treated CuAc film on silver electrodes when exposed to 300 ppb of H_2S for three hours. The plasma-treated sensor fabricated on gold/AuNP electrodes could also be regenerated by subsequent plasma treatments (Figure 31B). After the initial exposure to H_2S gas (1 ppm) and subsequent decrease in resistance, the sensor was again plasma treated for 2 minutes resulting in an increase of resistance of the sensor over 100 MΩ. The second exposure of the sensor towards 1ppm H_2S resulted again in almost seven orders of magnitude change in the resistance. The same procedure was repeated for the third time and similar results were observed showing the regeneration and reusability of the sensor by the plasma treatment. The regeneration did not significantly affect the saturation level reached after H_2S exposure. However, the detection rate of the sensor decreased somewhat after each regeneration cycle, t_{90} changing from 5 min (initial exposure) to 17 min after the first regeneration cycle and to 23 min after the second regeneration cycle.

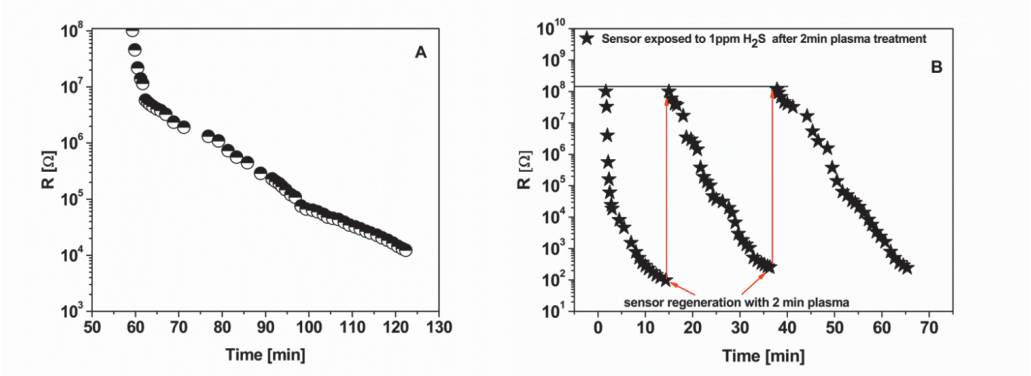

Figure 31. (A) Electrical response of the plasma treated sensor fabricated on gold/AuNP electrodes towards 300 ppb H_2S gas concentration at room temperature with 45% relative humidity. (B) Regeneration of the sensor by plasma after 1 ppm H_2S exposure.

The improvements on the H_2S gas sensing over the untreated CuAc film are suggested to be due to two possible mechanisms as shown in Figure 32. Firstly, the formation of p-type semiconducting Cu_2O (and its cross defect structure Cu_3O_2) through the plasma oxidation of CuAc film facilitates the growth of particles resulting in sufficient particle-particle contact prior to the exposure to H_2S gas (paper VI). Secondly, the oxidation of H_2S gas to sulfur by oxygen adatoms leads to the formation of a Cu_2O (Cu_3O_2)/Cu_xS core-shell structure where a thin layer of Cu_xS facilitates the rapid formation of a conductive percolation path between the electrodes. This leads to a decrease in resistance of the sensor with improved onset time and rate of detection compared to the untreated CuAc film. It has been previously shown that Cu_2O particles suspended in a Na_2S solution or exposed to low concentration of H_2S gas are immediately converted into Cu_2O/CuS core-shell structures at room temperature.[138, 139] Although the change in resistance upon H_2S exposure is irreversible at ambient conditions as illustrated in Figure 32, the sensor can be regenerated by oxidizing the thin Cu_xS layer to Cu_xO by plasma treatment. Furthermore, the incorporation of catalytic AuNPs in the sensing film improved the detection limit of the sensor to sub-ppm level at room temperature as shown in paper VI. These improvements enable the use of mass-manufacturable printed paper-based H_2S sensors in demanding applications needing very fast and sub-ppm detection.

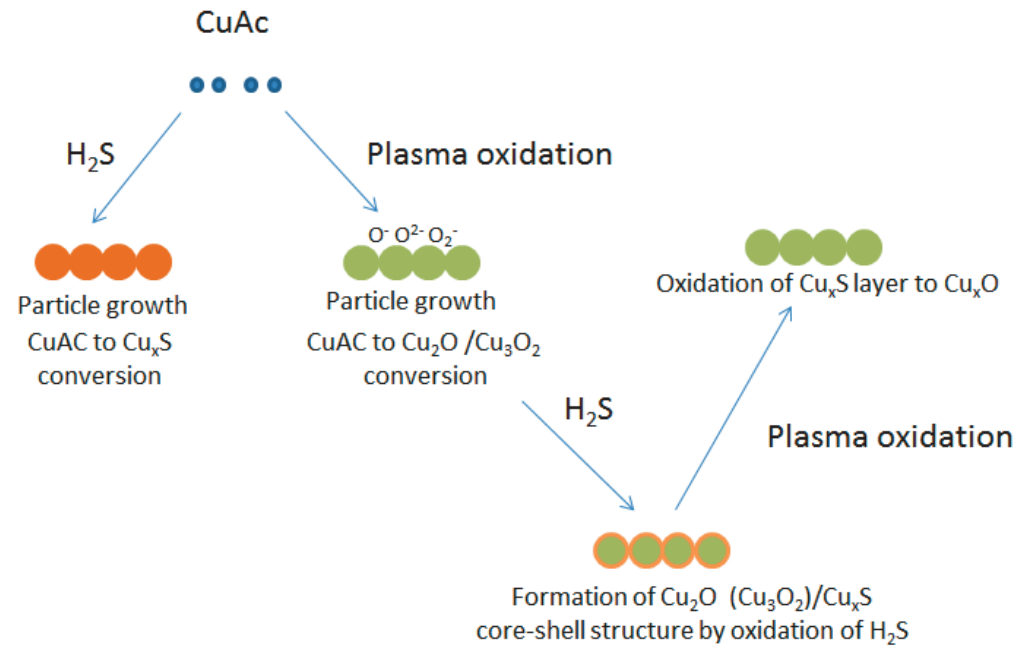

Figure 32. A schematic illustration of the effect of plasma treatment and exposure to H_2S on the structure of a copper acetate film.

5.6.12. Case study: wireless detection of biogenic H_2S

The usage of the developed CuAc based sensors for monitoring the quality of raw broiler meat by detecting the biogenic hydrogen sulphide as an end product of microbial metabolism was reported in paper VII. The rate of bacterial spoilage of raw poultry, in the manner of other microbiologically perishable foods, depends on the growth rate, concentration and metabolism of bacteria proliferating in food. Food is spoiled when the level of any bacterial metabolite exceeds the human sensory threshold. For raw poultry, it is often the sulphur containing bacterial metabolites that limits the shelf life time.[140, 141, 142] Under modified atmosphere packaging (MAP) conditions, hydrogen sulphide has been determined to be one of the prominent volatiles released during the spoilage of raw poultry.[140, 141, 142]

The response of paper-based sensors in the broiler meat box was studied both in aerobic (AIR) and anaerobic (MAP) conditions in storage during refrigeration (+6 °C) and at room temperature (RT). In addition, the suitability and function of two individual, printed electrode materials, Ag and Au, were tested and compared (paper VII).

The RLC sensors (PET based) were used to demonstrate the method for reading the sensor response wirelessly (Figure 33). The inductance of 2.1 μH for a rectangular planar antenna was calculated, based on the dimensional parameters of the coil. Similar coil dimensions were used for all the circuit variants. The capacitors were sized to be

65.6 pF and 179.4 pF, in order to achieve the operation frequencies of 13.56 MHz and 8.2 MHz, respectively. The above-mentioned frequencies were selected, because there are commercial readers available for these frequencies. By using a thickness of 27.5 µm for the two consecutive insulator layers and relative permittivity of 4.4 for the polymer dielectric, the practical resonant frequency of the manufactured circuits was typically below the target value but could easily be adjusted by mechanically decreasing the size of the upper capacitor plate. The finger gap and the size of the active area of the interdigitated sensor were also varied in the circuits. A commercial hand-held EAS (Electronics Article Surveillance) reader (Omni® verifier/deactivator, Checkpoint) was used for demonstrating the wireless reading of the RLC sensors. In our case, the RLC sensor is adjusted to a frequency of 8.2 MHz, and when moved into the vicinity of the reader's magnetic field, the reader gives an alarm. When the sensor resistance in the RLC circuit decreases due to H_2S exposure to a sufficiently low level, the quality factor (Q) of the circuit is lowered so that the reader does not recognize the circuit. The operation principle is demonstrated in Figure 33, where chip resistors were added between the sensor fingers (i.e. parallel with the sensor) to decrease the sensor resistance. The impedance was measured with an LCR-meter using a wired method. At the beginning, when no chip resistors were added and the resonant frequency was properly adjusted by modifying the capacitor, the EAS reader recognized the RLC sensor from the maximum distance of 7 cm. When resistors were added so that combined parallel resistances were 10 kΩ, 5 kΩ and 2.5 kΩ, the maximum reading distance decreased to 5 cm, 4 cm and 1 cm, respectively. When the combined resistance was 1.25 kΩ, the reader did not recognize the sensor anymore at any distance.

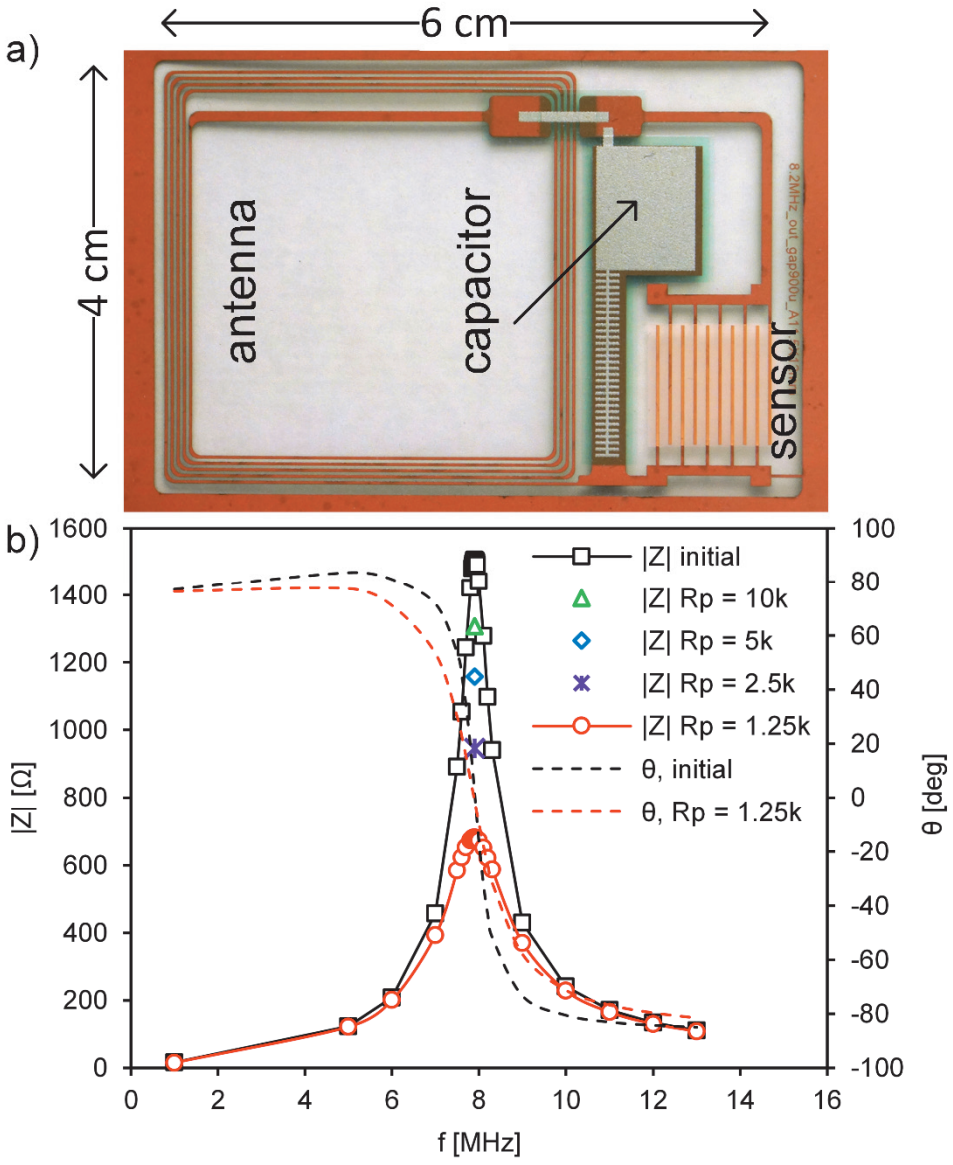

Figure 33.a. The RLC sensor structure used in the test, in which chip resistors were connected between sensor fingers to demonstrate the decrease of the sensor resistance and b) measured impedance change of the circuit. Only peak values are presented for measured impedances between the initial and final impedance curves.

Typical response curves of PET-based sensors in MAP/+6°C are presented in Figure 34. Compared to paper-based sensors, a negligible effect of humidity was observed with PET-based sensors, and the initial resistance value (>1 GΩ) was not markedly affected by the humidity. Because of the minimal humidity effect of the PET-based sensors, the H_2S-response can be detected earlier in relation to the use-by date. The earliest clear sensor response can be seen at 120 h (3.4 days after the use-by date;

sensor S2) when the resistance decreased to 300 kΩ. The initial capacitance values in Figure 34 were 1 – 3 pF: these values remained fairly stable during the entire test period and were not strongly affected by the humidity. Deviation in the capacitances of the three sensors can be explained by the differences in active areas of the sensors S1, S2 and S3 (11.5 × 12; 6 × 12 and 6 mm × 6 mm, respectively). All three sensors had a finger gap of 300 µm. The resistance of the sensors with an active area of 6 mm × 6 mm did not always decrease to a low enough value under H_2S exposure. The sensor with the size of the active area of 6 mm × 12 mm worked reliably and had the capacitance of 2 pF, which remained fairly stable until it dropped below the detection limit when the resistance of the sensor decreased below 100 Ω. Generally, the absolute capacitance value of the sensors with varying humidity values was considerably smaller in PET-based sensors than in paper-based sensors (paper VII). Thus, PET-based sensors were considered the better choice for RLC circuit operation.

It was not possible to read the RLC sensors wirelessly during the broiler meat tests, because the metal enclosure blocked the signal. A couple of RLC sensors were placed, however, inside the box, together with PET-based sensors. Before the tests, the EAS reader recognized the RLC sensors from a distance of 5–6 cm, but after the tests the reader did not recognize them anymore, proving that an on/off-type response to H_2S can be detected.

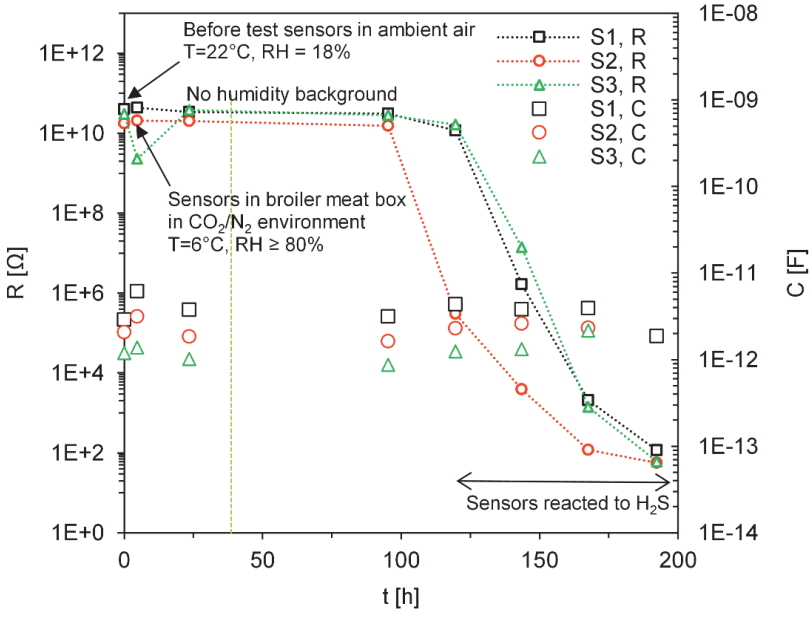

Figure 34. The resistance and capacitance measurements are shown as a function of time on the PET-based sensors in MAP at +6°C test. The (green) dotted vertical line indicates the end of the use-by day of the tested broiler meat batch.

The positive H_2S sensor responses in MAP at +6°C were associated with high levels (>108 CFU/g) of bacteria. The results show that the sensors can be used as a food quality indicator. In paper VII the sulfidation of the metal electrodes during exposure was prevented by using gold as the electrode material or by using a protective coating. The humidity effects on the sensor performance were considerably decreased by using a PET substrate for the sensors. A concept of a sensor platform in which the sensor was combined with a planar coil antenna and a capacitor to construct a wirelessly readable resonance circuit was presented in paper VII. The sensor is suitable for a commercial mass scale manufacturing process, which makes it inexpensive and hence capable of being integrated in a low-cost retail food package.

6. SUMMARY AND OUTLOOK

The main focus in this thesis was to develop a low cost H_2S gas sensor with significantly improved sensing parameters. Commercially available materials were modified and optimized for printability and H_2S gas sensing functionality. Printability is important since it enables the mass production of the sensors and thereby lowers the unit cost.

In paper I drop-casted deprotonated EB PANI/CC films were prepared on paper substrates containing inkjet-printed silver electrodes. These films showed large changes in the resistance ($>10^3$) upon exposure to low concentrations of H_2S (10ppm) at room temperature. These large changes in resistance were explained to arise from the formation of copper sulfide and concurrent protonation of PANI. While special morphologies of PANI (nano-fibers) have been used earlier as sensing films which have relatively large surface area for enhancing the H_2S gas sensitivity, we have demonstrated in paper I that by using a porous substrate like paper similar results can be achieved by conventional PANI through optimization of the PANI and metal salt concentration.

In paper II a fully printed H_2S sensor based on an aqueous dispersion of PANI/CC mixture was demonstrated. The sensing film was produced by screen printing or spray coating of the sensing material on interdigitated printed silver electrodes. The H_2S sensing functionality with respect to pH and metal salt concentration was optimized. The printed chemiresistors showed improved H_2S sensitivity compared to drop-casted films. One of the problems was the instability of the PANI/CC dispersion at the optimized pH. It was concluded that optimized PANI/CC dispersions (optimum with respect to H_2S sensitivity) were not suitable for roll-to-roll printing.

In paper III efforts were made to improve the stability of the PANI/CC dispersion. For this purpose a CC/CA mixture was used instead of CC. The addition of CA improved the overall stability of the dispersion without compromising the H_2S gas sensing functionality. Roll-to-roll printed films were made out of the stable dispersion using flexography and the H_2S gas sensing functionality of the sensors was verified.

It was realized that the use of PANI-based sensors in real life applications is limited due to their inherent sensitivity towards humidity and long-term instability. Because of these reasons another type of fully printed H_2S sensor based on CuAc was demonstrated (paper IV). The sensor showed several orders of magnitude change in resistance ($>10^8$) when exposed to 10 ppm of H_2S gas at room temperature. The effect of different solvents, film thickness and substrates (absorbing and nonabsorbing) were studied to optimize the sensor response. The large change in the resistance was concluded to be due to conversion of insulating CuAc particles to semi-metallic copper sulfide particles.

In paper V the performance of a printed CuAc based H_2S sensor was investigated. The sensor showed excellent sensitivity and long term stability, as well as negligible humidity effects and cross-sensitivity. It was concluded that the sensor can be utilized for quantitative detection of H_2S within the range of 1 - 20 ppm.

In paper VI it was shown that the sensitivity and the lower limit of detection of the CuAc based H_2S sensor can be significantly improved by incorporation of catalytic gold nanoparticles and surface plasma treatment. The modified sensor was capable to detect sub-ppm levels of H_2S at room temperature.

In paper VII a demonstration of wireless detection of biogenic H_2S produced by the degradation of poultry meat using a CuAc based H_2S sensor was shown. It was concluded that the sensor can be integrated in an RLC circuit to generate a wireless signal upon interaction with the H_2S gas. It was observed that at high humidity conditions silver electrodes degrades when exposed to H_2S for long exposure times (> 2 - 3 h) and can be considered to be a suitable electrode material only when dealing with short H_2S exposures.

Copper sulfide is a very interesting material and is applied in for example biomedical and sensing applications, photovoltaics etc. Currently much research is carried out on the use of copper sulfide based materials in bio-medical applications like photothermal ablation, photoacoustic imaging, drug delivery, theranostics etc. It can also be employed for the detection of DNA, glucose and amines. Future prospects include the development of a new generation of copper sulfide based sensors for basic and volatile biogenic amines. Copper sulfide forms stable complexes with amines at room temperature. The main challenge foreseen here is to develop a sensor which is selective towards different classes of amines.

7. REFERENCES

[1] G. Wang, Modification of vapor sensitivity in ellipsometric gas sensing by copper deposition in Porous Silicon, Sensors and Actuators B, 4263 (2002) 1.

[2] S. Zangooie, R. Bjorklund, H. Arwin, Vapor Sensitivity of thin porous silicon layers, Sensors and Actuators B, 43 (1997) 168.

[3] L. Pancheri, C. Oton, Z. Gaburro, G. Soncini, L. Pavesi, Very sensitive porous silicon NO_2 sensor, Sensors and Actuators B, 6974 (2003) 1.

[4] J. Gole, J. DeVincentis, L. Seals, P. Lillenhei, S. Prokes, D. Dickson, Chloride salt enhancement and stabilization of the photoluminescence from a porous silicon surface, Physical Review B, 61 (2000) 5615.

[5] S. Prokes, W. Carlos, L. Seals, J. Gole, Defect study of light-emitting HCl-treated porous silicon, Physical Review B, 62 (2000) 1878.

[6] J. Gole, L. Seals, P. Lillehei, Patterned metallization of porous silicon from electroless solution for direct electrical contact, Journal of the Electrochemical Society, 147 (2000) 3785.

[7] Hazardous Substances Databank (HSDB), Hydrogen sulfide: Environmental Fate & Exposure, National Library of Medicine, Bethesda, MD, USA, 2011 (http://toxnet.nlm.nih.gov/cgi-bin/sis/search/f?./temp/~4DMpSO:1, accessed on 19 January 2011).

[8] Occupational Safety and Health Administration (OSHA), Fact sheet of Hydrogen sulfide (H_2S), DSG 10/2005 (http://www.osha.-gov/OshDoc/data_Hurricane_Facts/hydrogen_sulfide_fact.pdf).

[9] J. Sarfraz, D. Tobjork, R. Osterbacka, and M. Linden, Low-Cost hydrogen sulfide gas sensor on paper substrates: fabrication and demonstration, IEEE Sensors Journal, 12 (2012) 1973.

[10] R.O. Beauchamp, J.S. Bus, J.A. Popp, C.J. Boreiko, D.A. Andjelkovich, P. Leber, A critical review of the literature on hydrogen sulfide toxicity, CRC Critical Review in Toxicology, 13 (1984) 25.

[11] K. Crowley, E. O'Malley, A. Morrin, M. R. Smyth and A. J. Killard, An aqueous ammonia sensor based on an inkjet-printed polyaniline nanoparticle-modified electrode, Analyst, 133 (2008) 391.

[12] N.E. Agbor, M.C.Petty, A.P.Monkman, Polyaniline thin film for gas sensing, Sensors and Actuators B, 28 (1995) 173.

[13] S. Sharma, C. Nirkhe, S. Pethkar, A. A. Athawale, Chloroform vapor sensor based on copper/polyaniline nano composite, Sensors and Actuators B, 85 (2002) 131.

[14] N. Densakulpraserta, L. Wannatonga, D. Chotpattananonta, P. Hiamtupa, A. Sirivata, J. Schwankb, Electrical conductivity of polyaniline/zeolite composites and synergetic interaction with CO, Materials Science and Engineering B, 117 (2005) 276.

[15] M. Vilkman, K. Lehtinen, T. Mäkelä, P. Rannou, O. Ikkala, Polyaniline doped with 5-formyl-2-furansulfonic acid a humidity memory, Organic Electronics, 11 (2010) 472.

[16] X. Ma, M. Wang, H. Chen, G. Li, J. Sun, and R. Bai, Preparation of water soluble PANI and its gas sensitivity, Green Chemistry, 7 (2005) 507.

[17] J. Fraden. Handbook of modern sensors: Physics, designs and applications. AIP Press, second edition, 1997.

[18] H. A. Schultens and D. Schild, Biophysical properties of olfactory receptor neurones, chapter 2, 13-23. In Gardner and Bartlett, 150 (1992). NATO ASI Series. Series E: Applied Sciencies 212.

[19] R. Berne and M. Levy, editors. Principles of physiology, Wolfe Publications, 1990.

[20] J. W. Gardner and P. N. Bartlett, Pattern recognition in odour sensing, chapter 11, 161-179. In Gardner and Bartlett, 150 (1992). NATO ASI Series. Series E: Applied Sciencies 212.

[21] https://classconnection.s3.amazonaws.com/418/flashcards/93418/jpg/picture22133839594805 2.jpg.

[22] https://classconnection.s3.amazonaws.com/184/flashcards/1904184/jpg/41352650358237.jpg.

[23] José Miguel Alves Correia Pires, Ph.D. Thesis, Thin films for gas sensors, Departamento de Física Universidade do Minho (2003).

[24] Z. Yunusa, M. Hamidon, A. Kaiser, Z. Awang, Gas sensors: A review, Sensors & Transducers, 168 (2014) 61.

[25] X.S. Liang, Y.H. He, F.M. Liu, B. Wang, T.G. Zhong, B. Quan, G. Lu, Solid-state potentiometric H_2S sensor combining NASICON with Pr_6O_{11}-doped SnO_2 electrode, Sensors and Actuators B, 125 (2007) 544.

[26] http://www.ngk.de/en/products-technologies/lambda-sensors/lambda-sensor-technologies/zirconium-dioxide-lambda-sensor/.

[27] T. Hübert, L. Boon-Brett, G. Black, U. Banach, Hydrogen sensors - A review, Sensors and Actuators B, 157 (2011) 329.

[28] J.R Stetter, J. Li, Amperometric gas sensors a review, Chemical Reviews, 108 (2008) 352.

[29] G. Korotcenkov, S. Han, J. R. Stetter, Review of Electrochemical Hydrogen Sensors, Chemical Reviews, 109 (2009) 1402.

[30] Y. Wang, H. Yan, E.F. Wang, The electrochemical oxidation and the quantitative determination of hydrogen sulfide on a solid polymer electrolyte-based system, Journal of Electroanalytical Chemistry, 497 (2001)163.

[31] G.F. Fine, L.M. Cavanagh, A. Afonja, R. Binions, Metal Oxide Semi-Conductor Gas Sensors in Environmental Monitoring, Sensors, 10 (2010) 5469.

[32] J.R. Stetter, W.R. Penrose, S. Yao, Sensors, Chemical Sensors, Electrochemical Sensors, and ECS, Journal of the Electrochemical Society, 150 (2003) 11.

[33] T.C. Pearce, S. Schiffman, H. Nagle, and J. Gardner, (2003), Handbook of Machine Olfaction, Wiley-VCH, Weinheim.

[34] K. J. Albert, N. S. Lewis, C.L. Schauer, G. A. Sotzing, S. E. Stitzel, T. P. Vaid, and D. R. Walt, Cross reactive chemical sensor arrays, Chemical Reviews, (2000) 2595.

[35] E. Schaller, J. Bosset and F. Escher, Electronic noses and their application to food, Lebensmittel-Wissenschaft und-Technologie, 31 (1998) 305.

[36] A. Galdikas, A. Mironas, A. Šetkus, Copper doping level effect on sensitivity and selectivity of tin oxide thin-film gas sensor, Sensors and Actuators B,: Chemical, 26 (1995) 29.

[37] C. Wang, L. Yin, L. Zhang, D. Xiang and R. Gao, Metal Oxide Gas Sensors: Sensitivity and Influencing Factors, Sensors, 10 (2010) 2088.

[38] Y. Lu, J. Li, J. Han, H. Ng, C. Binder, C. Partridge, M. Meyyappan, Room temperature methane detection using palladium loaded single-walled carbon nanotube sensors, Chemical Physics Letter, 391 (2004) 344.

[39] D. Wang, Z. Ma, S. Dai, J. Liu, Z. Nie, M. Engelhard, Q. Huo, C. Wang and R. Kou, Low-Temperature Synthesis of Tunable Mesoporous Crystalline Transition Metal Oxides and Applications as Au Catalyst Supports, The Journal of Physical Chemistry C, 112 (2008) 13499.

[40] D. Haridas, K. Sreenivas, V. Gupta, Improved response characteristics of SnO_2 thin film loaded with nanoscale catalysts for LPG detection, Sensors and Actuators B, 133 (2008) 270.

[41] A. Chaturvedi, V. Mishra, R. Dwivedi, S. Srivastava, Response of oxygen plasma-treated thick film tin oxide sensor array for LPG, CCl_4, CO and C_3H_7OH, Microelectronics Journal, 30 (1999) 259.

[42] R. Srivastava, R. Dwivedi, S. Srivastava, Development of high sensitivity tin oxide based sensors for gas/odour detection at room temperature, Sensors and Actuators B, 50 (1998) 175.

[43] S. Virji, J.D. Fowler, C.O. Baker, J. Huang, R.B. Kaner, B.H. Weiller, Polyaniline Nanofiber Composites with Metal Salts: Chemical Sensors for Hydrogen Sulfide, Small, 1 (2005) 624.

[44] M.D. Shirsat, M.A. Bangar, M.A. Deshusses, N.V. Myung, A. Mulchandani, Polyaniline nanowires-gold nanoparticles hybrid network based chemiresistive hydrogen sulfide sensor, Applied Physics Letters, 94 (2009) 083502.

[45] C. McDonagh, C.S. Burke, B.D. MacCraith, Optical Chemical Sensors, Chemical Reviews, 108 (2008) 400.

[46] Sudhir Kumar Pandey, Ki-Hyun Kim, Kea-Tiong Tang, A review of sensor-based methods for monitoring hydrogen sulfide, Trends in Analytical Chemistry, 32 (2012) 87.

[47] A.W. Czanderna, T.M. Thomas, A Quartz Crystal Microbalance Apparatus for Water Sorption by Polymers, Journal of Vacuum Science and Technology, 5 (1987) 2412.

[48] X. Wang, B. Ding, J. Yu, M. Wang, F. Pan, A highly sensitive humidity sensor based on a nanofibrous membrane coated quartz crystal microbalance, Nanotechnology, 21 (2010) 055502.

[49] T.B. Pollard, T.D. Kenny, J.F. Vetelino, M.P. da Cunha, Pure SH-SAW Propagation, Transduction and Measurements on $KNbO_3$, IEEE Transactions on Ultrasonics, Ferroelectrics, and Frequency Control, 53 (2006) 199.

[50] O. Tigli, M.E. Zaghloul, A Novel Saw Device in CMOS: Design, Modeling, and Fabrication, Sensors Journal, IEEE, 7 (2007) 219.

[51] M. Gomes, P. Nogueira, J. Oliveira, Quantification of CO_2, SO_2, NH_3 and H_2S with a single coated piezoelectric quartz crystal, Sensors and Actuators B, 68 (2000) 218.

[52] R.S. Falconer, I.F. Vetelino, D.J. Smith, M.J. Osbom, an Activation Process for Increased Sensitivity of a SAW Gas Microsensor, IEEE Ultrasonic. Symposium, (1990).

[53] T. Ishihara and S. Matsubara, Capacitive Type Gas Sensors, Journal of Electroceramics, 2 (1998) 215.

[54] E. Traversa, Ceramic sensors for humidity detection: the state-of-the-art and future developments, Sensors and Actuators B, 23 (1995) 135.

[55] K. Domansky, J. Liu, L.-Q. Wang, M. H. Engelhard and S. Baskaran, Chemical sensors based on dielectric response of functionalized mesoporous silica films, Journal of Materials Research, 16 (2001) 2810.

[56] J. G. Firth, A. Jones, T. Jones, The principles of the detection of flammable atmospheres by catalytic devices, Combustible Flame, 20 (1973) 303.

[57] E. Jones, The pellistor catalytic gas detection, in: P.Moseley, B. Tofield (Eds.), Solid State Gas Sensors, Adam Hilger, Bristol Chapter 2 (1987) 17

[58] W. Shin, M. Matsumiya, N. Izu, and N. Murayama, Hydrogen-selective thermoelectric gas sensor, Sensors and Actuators B: Chemical, 93 (2003) 304.

[59] W. Shin, M. Matsumiya, F. Qiu, N. Izu, and N. Murayama, Thermoelectric gas sensor for detection of high hydrogen concentration, Sensors and Actuators B: Chemical, 97 (2004) 344.

[60] K.D. Benkstein, S. Semancik, Mesoporous nanoparticle TiO_2 thin films for conductometeric gas sensing on micro hotplate platforms, Sensors and Actuators B, 113 (2006) 445.

[61] G.T. Barnes, I.R. Gentle, Interfacial science, Oxford University Press (2005).

[62] J. Lyklema, Points of zero charge in the presence of specific adsorption, Colloid and interface science, 99 (1984) 109.

[63] J. Lyklema, Fundamentals of Interface and Colloid Science, 2, Academic press (1991).

[64] R.J. Pugh, L. Bergstrom, Surface and colloid chemistry in advanced ceramic processing, CRC Press, 51 (1994) 97.

[65] D. J. Shaw, Introduction to colloid and surface chemistry Butterworths 3rd ed. 148.

[66] P.C. Hiemenz., R. Rajagopalan. Principles of colloid and surface chemistry, CRC Press 3rd edition (1997).

[67] http://www.malverninstruments.co.kr/LabEng/industry/colloids/dlvo_theory_2.jpg (5th jan 2009).

[68] J. Lyklema, Fundamentals of Interface and Colloid Science, Academic Press 1 (1991) 1.

[69] http://www.malvern.co.uk/LabFre/industry/colloids/Stabilization.gif(8 jan 2009).

[70] R. Bollström, M. Tuominen, A. Määttänen, J. Peltonen, M. Toivakka, Top layer coatability on barrier coatings, Progress in Organic Coatings, 73 (2012) 26.

[71] R. Bollström, A. Määttänen, P. Ihalainen, J. Peltonen, M. Toivakka, Patent application PCT/FI2010/050056, WO 2010/086511.

[72] R. Bollström, J. Saarinen, J. Räty and M. Toivakka, Measuring solvent barrier properties of paper, Measurement science and technology, 23 (2012) 015601.

[73] H. Juvonen, A. Määttänen, P. Laurén, P. Ihalainen, A. Urtti, M. Yliperttula, J. Peltonen, Biocompatibility of printed paper-based arrays for 2-D cell cultures, Acta Biomaterialia, 9 (2013) 6704.

[74] M.Ostwal, Experimental amd atomistic simulation studies of water sorption in polyaniline, University of Southern California, 2007.

[75] C. K. Chiang, C. R. Fincher, Jr., Y. W. Park, A. J. Heeger, H. Shirakawa, E. J. Louis, S. C. Gau, and Alan G. MacDiarmid, Electrical conductivity in doped polyacetylene, Physical Review Letters, 39 (1977) 1098.

[76] B. Lesiak, A. Jablonski, J. Zemek, M. Trchová, and J. Stejskal, Determination of the inelastic mean free path of electrons in different polyaniline samples, Langmuir, 16, (2000) 1415.

[77] E. Song and J. Choi, Conducting polyaniline nanowire and its applications in chemiresistive sensing, Nanomaterials, 3 (2013) 498.

[78] S. Bhadra, D. Khastgir, N. Singha, J. Lee, Progress in preparation, processing and

applications of polyaniline, Progress in Polymer Science, 34 (2009) 783.

[79] B. He, Q. Tang, T. Liang and Q. Li, Efficient dye-sensitized solar cells from polyaniline–single wall carbon nanotube complex counter electrodes, Journal of Materials Chemistry A, 2 (2014) 3119.

[80] F. Kelly, L. Meunier, C. Cochrane, V. Koncar, Polyaniline: Application as solid state electrochromic in a flexible textile display, Displays, 34 (2013) 1.

[81] M. Hostetler, J. Wingate, C. Zhong, J. Harris, R. Vachet, M. Clark, J. Londono, S. Green, J. Stokes, G. Wignall, G. Glish, M. Porter, N. Evans, and R. Murray, Alkanethiolate Gold Cluster Molecules with Core Diameters from 1.5 to 5.2 nm: Core and Monolayer Properties as a Function of Core Size, Langmuir, 14 (1998) 17.

[82] A. Määttänen, P. Ihalainen, P. Pulkkinen, S. Wang, H. Tenhu, & J. Peltonen, Inkjet-Printed Gold Electrodes on Paper: Characterization and Functionalization, ACS Applied Materials and Interfaces, 4 (2012) 955.

[83] A. Määttänen, U. Vanamo, P. Ihalainen, P. Pulkkinen, H. Tenhu, J. Bobacka, & J. Peltonen, A low-cost paper-based inkjet-printed platform for electrochemical analyses, Sensors and Actuators B, 177 (2013) 153.

[84] D. Tobjörk, Printed low-voltage organic transistors on plastic and paper, PhD. Thesis, Åbo Akademi University (2012).

[85] E. Tekin, P. Smith and U. Schubert, Inkjet printing as a deposition and patterning tool for polymers and inorganic particles, Soft matter, 4 (2008) 703.

[86] M. Singh, H. Haverinen, P. Dhagat and G. Jabbour, Inkjet printing - Process and its applications, Advanced Materials, 22 (2010) 673.

[87] L. Yang, R. Zhang, D. Staiculescu, C. P. Wong and M. Tentzeris, A novel conformal RFID-enabled module utilizing inkjet-printed antennas and carbon nanotubes for gas detection applications, IEEE Antennas and Propagation Society, 8 (2009) 653.

[88] R. Bollström, Paper for printed electronics and functionality, PhD. Thesis, Åbo Akademi University (2013).

[89] D. Shin, Y. Lee, C. Kim, Performance characterization of screen printed radio frequency identification antennas with silver nanopaste, Thin solid films, 517 (2009) 6112.

[90] F. Krebs, M. Jørgensen, K. Norrman, O. Hagemann, J. Alstrup, T. Nielsen, J. Fyenbo, K. Larsen, J. Kristensen, A complete process for production of flexible large area polymer solar cells entirely using screen printing-First public demonstration, Solar Energy Materials and Solar Cells, 93 (2009) 422.

[91] J. Sarfraz, P. Ihalainen, A. Määttänen, J. Peltonen, M. Lindén, Printed hydrogen sulfide gas sensor on paper substrate based on polyaniline composite, Thin Solid Films, 534 (2013) 621.

[92] M. Salomäki, T. Peltonen, J. Kankare, Multilayer films by spraying on spinning surface — Best of both worlds, Thin Solid Films, 520 (2012) 5550.

[93] D. Briggs, M. Seah., Eds.; In Practical Surface Analysis, Volume 1, Auger and X-ray Photoelectron Spectroscopy; Wiley (1994).

[94] D. Briggs, Applications of XPS in polymer technology, in practical surface analysis by Auger and X-ray photoelectron spectroscopy, 2nd Ed., D. Briggs and M. P. Seah, eds. (Wiley, London, 1990) 437.

[95] S. Zhang, S. Zhang, L. Li, A. Kumar, Materials characterization technique, CRC press, Taylor and Francis group (2009).

[96] L. Reimer, Elements of a transmission electron microscope, Springer Berlin (1993).

[97] FEI company, PDF: Introduction to electron microscopy, URL: www.fei.com/documents/introduction-to-microscopy-document.

[98] M. Järn, Influence of topography and surface chemistry on wetting properties of TiO_2-based ceramic coatings, PhD. Thesis, Åbo Akademi University (2010).

[99] Q. Zhong, D. Inniss, K. Kjoller, V. Elings, Fractured polymer silica fiber surface studied by tapping mode atomic force microscopy, Surface Science, 290 (1993) 688.

[100] Image Metrology, the scanning probe image processor, SPIP™, User and reference guide version 4.4.2007.

[101] D. Debarnot and F. Epaillard, Polyaniline as a new sensitive layer for gas sensors, Analytica Chimica Acta, 475 (2003) 1.

[102] A. MacDiarmid, Synthetic Metals: A novel role for organic polymers (Nobel Lecture) Angewandte Chemie International Edition, 40 (2001) 2581.

[103] O. Ngamna, A. Morrin, A. Killard, S. Moulton, M. Smyth, and G. Wallace, Inkjet printable polyaniline nanoformulations, Langmuir, 23 (2007) 8569.

[104] C. Deslouis, T. El Moustafid, M. M. Musiani, M. E. Orazem, V. Provost and B. Tribollet, Effect of cations on the diffusivity of the charge carriers in polyaniline membranes, Electrochimica Acta, 44 (1999) 2087-2093.

[105] G. Inzelt and G. Horanyi, Some problems connected with the study and evaluation of the effect of pH and electrolyte concentration on the behaviour of polyaniline film electrode, Electrochimica Acta, 35 (1990) 27.

[106] M. Pitluck, B. Pollard, D. Haworth, Determination of stability constants of a copper/citric acid complex by ion-exchange chromatography and atomic absorption spectrometry, Analytica Chimzca Acta, 197 (1987) 339.

[107] R. W. Parry , F. W. DuBois, Citrate Complexes of Copper in Acid Solutions, Journal of the American Chemical Society, 74 (1952) 3749.

[108] T. Field, J. McCourt, W. McBryde, Composition and stability of iron and copper citrate complexes in aqueous solution, Canadian Journal of Chemistry, 52 (1974) 3119.

[109] G. Graffmann, H. Domels, and M. L. Sträter, Schnelle bestimmung von citrat in wasch- und reinigungsmitteln durch titration mit cu-lösung, fette, Seifen, Anstrichmittel, 76 (1974) 218-220.

[110] C. J. Knuth and A. Bavley, Plastic Technology. 3 (1957) 555.

[111] A. J. Francis, C. J. Dodge, and J. B. Gillow, Biodegradation of metal citrate complexes and implications for toxic-metal mobility, Nature, 356 (1992) 140.

[112] J. Huang, S. Virji, B. H. Weiller, and R. B. Kaner, Nanostructured PANI Sensors, Chemistry A European Journal, 10 (2004) 1314.

[113] B. Abeles, H. Pinch, and J. Gittleman, Percolation conductivity in W-Al_2O_3 granular metal films, Physical Review Letters, 35 (1975) 247.

[114] P. Sheng, B. Abeles, and Y. Arie, Hopping conductivity in granular metals, Physical Review Letters, 31 (1973) 44.

[115] J. Moulder, W. Stickle, P. Sobol, K. Bomben, Hand book of X-ray photoelectron spectroscopy, 2nd edition, edited by J. Chastain (Perkin Elmer Coorporation, Physical Electronics, 1992) and references therein.

[116] B. Strohmeier, D. Levden, R. Field, D. Hercules, Surface spectroscopic characterization of Cu Al_2O_3 catalysts, Journal of Catalysis, 94 (1985) 514.

[117] N. Kuramoto, A. Tomita, Aqueous polyaniline suspensions: chemical oxidative polymerization of dodecylbenzenesulfonic acid aniline salt, Polymer, 38 (1997) 3055.

[118] V. Bhide, S. Salkalachen, A. Rastog, C. Rao, and M. Hegde, Depth profile composition studies of thin film CdS:Cu_2S solar cells using XPS and AES, Journal of Physics D: Applied Physics, 14 (1981) 1647.

[119] J. Klein, C. Li, D. Hercules, and J. Black, Decomposition of Copper Compounds in X-Ray Photoelectron Spectrometers, Applied Spectroscopy, 38 (1984) 729.

[120] G. Olafsdottir, R. Jonsdottir, H. Lauzon, J. Luten, and K. Kristbergsson, Characterization of volatile compounds in chilled cod (Gadus morhua) fillets by gas chromatography and detection of quality indicators by an electronic nose, Journal of Agricultural and Food Chemistry, 53 (2005) 10140.

[121] M. Zhao, X. Wang, L. Ninga, J. Jia , X. Li , L. Cao, Electrospun Cu-doped ZnO nanofibers for H_2S sensing, Sensors and Actuators B, 156 (2011) 588.

[122] D. Chavan, V. Gaikwad, G. Patil, D. Kajale, G. Jain, CdO doped indium oxide thick film as a low temperature H_2S gas sensor, Sensors and Transducers Journal, 129 (2011) 122.

[123] S. Virji, R. Kaner, and B. Weiller, Direct electrical measurement of the conversion of metal acetates to metal sulfides by hydrogen sulfide, Inorganic Chemistry, 45 (2006) 10467.

[124] D. Skoog, West, D.M. Analytical Chemistry, an introduction; Holt, Rinehart and Winston: New York, (1965).

[125] K. Osakada, A. Taniguchi, E. Kubota, S. Dev, K. Tanaka, K. Kubota, and T. Yamamoto, New organosols of copper(II) sulfide, cadmium sulfide, zinc sulfide, mercury(II) sulfide, nickel(II) sulfide and mixed metal sulfides in N,N-dimethylformamide and dimethyl sulfoxide. Preparation, characterization, and physical properties, Chemistry of Matererials, 4 (1992) 562.

[126] K.E. Somolyakova, Ref. Zh., Khim. 204 (1971) 236.

[127] B. Abeles, H.L. Pinch, and J.I. Gittleman, Percolation Conductivity in W-Al_2O_3 Granular Metal Films Physical Review Letters, 35, (1975) 247.

[128] Z. Nan, X. Wang, Z. Zhao, Formation of various morphologies of copper sulfides by a solvothermal method, Journal of Crystal Growth, 295 (2006) 92.

[129] S. Goh, A. Buckley, R. Lamb, Copper(II) sulfide? Minerals Engineering, 19 (2006) 204.

[130] J. Haber, T. Machej, L. Ungier, and J. Ziółkowski, ESCA studies of copper oxides and copper molybdates, Journal of Solid State Chemistry, 25 (1978) 207.

[131] X. Yu, F. Liu, Z. Wang, Y. Chen, Auger parameters for sulfur-containing compounds using a mixed aluminum-silver excitation source, Journal of Electron Spectroscopy and Related Phenomena**,** 50 (1990) 159.

[132] J. Sarfraz, A. Määttänen, P. Ihalainen, M. Keppeler, M. Lindén, J. Peltonen, Printed copper acetate based H_2S sensor on paper substrate, Sensors and Actuators B, 173 (2012) 868.

[133] P. Meester, S. Fletcher and A. Skapski, Refined crystal structure of tetra-μ-acetato-bisaquodicopper(II), Journal of the Chemical Society, Dalton Transactions**,** 23 (1973) 2575.

[134] G. Barclay and C. Kennard, The crystal structure of monopyridinecopper(II) acetate, Journal of Chemical Society, (1961) 5244.

[135] F. Hannic, D. Stempiova and K. Hanicova, The crystal structure of monopyridinecopper(II) acetate, Acta CrystalIographica, 17 (1964) 633.

[136] G. Davcy and F. Stephens, Crystal and molecular structure of mono-α-picolinecopper(II) chloroacetate, Journal of the Chemical Society A: Inorganic, Physical, Theoretical, (1970) 2803.

[137] P. Sullivan, J. Barbour, A. Missert, R. Copeland, M. Mayer, J. Campin, The effects of varying humidity on copper sulfide film formation, in: SAND Report, SAND2004-0670, (2004).

[138] S. Jiao, L. Xu, K. Jiang, D. Xu, Well-defined non-spherical copper sulfide mesocages with single-crystalline shells by shape-controlled crystal templating, Advanced Materials, 18 (2006) 1174.

[139] P. Wijesundara, D. Perera, D. Jayasuriya, W. Siripala, L. De Silva, P. Samantilleke, M. Dharmadasa, Sulphidation of electrodeposited cuprous oxide thin films for photovoltaic applications, Solar Energy Materials & Solar Cells, 61 (2000) 277.

[140] L. Freeman, G. Silverman, P. Angelini, C. Merritt, W. Esselen, Volatiles produced by microorganisms isolated from refrigerated broiler at spoilage, Applied and Environmental Microbiology, 32 (1976) 222.

[141] S. Viehweg, R. Schmitt, W. SchmidtLorenz, Microbial spoilage of refrigerated fresh broilers, Part VII, Production of off odours from poultry skin by bacterial isolates, Lebensm.-Wiss. Technol, 22 (1989) 356.

[142] M. Eilamo, A. Kinnunen, K. Latva-Kala, R. Ahvenainen, Effects of packaging and storage conditions on volatile compounds in gas-packed poultry meat, Food Additives and Contaminants, 15 (1998) 217.

ISBN 978-952-12-3251-0